NTNU – Trondheim
Norwegian University of
Science and Technology

Removal of SO2 from Flue Gas

Study of the Regenerable Labsorb Process

Ida Mortensen Bernhardsen

Chemical Engineering and Biotechnology
Submission date: June 2015
Supervisor: Magne Hillestad, IKP

Norwegian University of Science and Technology
Department of Chemical Engineering

Preface

This thesis is a result of the work conducted at Norwegian University of Science and Technology (NTNU) during fall 2015. It was carried out in the subject TKP4900, Environmental Engineering and Reactor Technology, at the department of Chemical Engineering (IKP) and completed the final semester at the master program Chemical Engineering and Biotechnology. In this work, the simulation program ASPEN Plus version 8.6 was used, along with the Mathworks numerical computing program MATLAB version R2014b.

I would like to thank Magne Hillestad for being my supervisor and Hanna Knuutila for all valuable guidance, feedback and support throughout the semester.

"I declare that this is an independent work according to the exam regulations of the Norwegian University of Science and Technology (NTNU)."

Trondheim, 2015-11-06

_____

Ida Bernhardsen

Abstract

Sulphur dioxide (SO_2) is a well-known air pollutant, and is primarily formed as a by-product when fossil fuels are burned at power plants. Due to stringent emission regulations, well-designed and efficient flue gas desulphurization technologies (FGD) are a necessity. One potential FGD technology is the regenerable Labsorb process. However, the process is little applied and limited information is available in the literature from plants, which have installed the process in full scale, pilot scale tests and laboratory studies.

This thesis seeks to find an electrolyte Non-Random Two Liquid (eNRTL) thermodynamic model in ASPEN Plus that is able to represent the experimental vapour-liquid equilibrium (VLE) data of the sodium-phosphate-water-SO_2-system. Thereafter, the model will be used to identify energy efficient operating conditions in the Labsorb process.

In the work to find a suitable eNRTL-model, binary interaction parameters were fitted to VLE data. Absorption and regeneration of SO_2 in the Labsorb process were simulated separately in ASPEN Plus. The Buffer 3/1/0.5, i.e. $C_{Na_2HPO_4}$=3 mol/L, $C_{NaH_2PO_4}$=1 mol/L and $C_{Na_2SO_4}$=0.5 mol/L was used as a solvent in the simulations.

In this work, it was developed an eNRTL model with an average deviation of 16.8% from experimental VLE data. The model was found to be valid in the temperature range 40 °C to 70 °C and in the SO_2 concentration range 0.5 mol_{SO2}/L to 1.6 mol_{SO2}/L for buffer 3/1/0.5. Furthermore, it was shown that the method used to improve VLE in ASPEN Plus works. When absorption of SO_2 was simulated, it was found that the absorption most likely was too ideal as it showed some deviation from available operating data. When regeneration of SO_2 was simulated, it was not possible to conclude which operating conditions were most energy efficient. The main challenge in the study was lack of experimental data.

Sammendrag

Utslipp av svoveldioksid (SO_2) er en viktig årsak til luftforurensning. SO_2, dannes hovedsakelig som et biprodukt når fossilt brensel forbrennes i et kraftverk. På grunn av strenge utslippskrav er veldesignede og energi effektive røykgass avsvovling teknologier (FGD) en nødvendighet. En mulig FGD teknologi er den regnererbare Labsorb prosessen. Imidlertid, prosessen er lite anvendt og begrenset informasjon er tilgjengelig i litteraturen fra anlegg, som har installert prosessen i fullskala, fra tester som er gjort på pilotanlegg og fra laboratorie studier.

Denne oppgaven går ut på å finne en elektrolytt ikke-randomisert to væske (eNRTL) termodynamisk modell i ASPEN Plus som er i stand til å representere eksperimentelle gass-væske-likevekt (VLE) data for natrium-fosfat-vann-SO_2-systemet. Modellen skal så benyttes til å finne energieffektive arbeidsbetingelser i Labsorb prosessen.

I arbeidet med å finne en egnet eNRTL-modell, ble binære interaksjoner justert ved hjelp av VLE data. Absorpsjon og regenerering av SO_2 i Labsorb prosessen ble simulert separat i ASPEN Plus. Buffer 3/1/0.5, dvs. $C_{Na_2HPO_4}$ =3 mol/L, $C_{NaH_2PO_4}$ =1 mol/L og $C_{Na_2SO_4}$ =0.5 mol/L ble benyttet som solvent i simuleringen.

I denne oppgaven ble det utviklet en eNRTL modell med et gjennomsnittlig avvik på 16.8 % fra eksperimentelle VLE data. Modellen er gyldig i temperaturområdet 40 °C til 70 °C og i SO_2 konsentrasjonsområdet 0.5 mol_{SO2}/L til 1.6 mol_{SO2}/L for buffer 3/1/0.5. Videre ble det vist at fremgangsmåten som brukes for å forbedre VLE i ASPEN Plus fungerer. Ved simulering av absorpsjon av SO_2 ble det funnet at absorpsjonen mest sannsynlig var for ideell da den ikke var direkte sammenlignbar med innsamlede driftsdata. Ved simulering av regenerering av SO_2 var det ikke mulig å konkludere hvilke driftsbetingelser som var mest energieffektive. Den største begrensningen og utfordringen i oppgaven var mangel på eksperimentelle data.

Contents

List of Symbols

A, B, C, D, E, F, G, k	Parameter	
A_{φ}	Debye-Hückel parameter	
a	Activity	
C_i	Concentration of component I	mol/L
C_i	Ci=zi for ionic species, and Ci=1 for molecular species	
f	Fugacity	
d	Density	g/cm^3
G	Gibbs energy	J/mol
H	Henrys constant	kPa
I_x	Ionic strength	mol/L
k_B	Boltzmann constant	J/K
M	Molecular weight	g/mol
N	Number of data points	
N_A	Avogadro's number	mol^{-1}
n	Mole flow	mol/hr
P	Pressure	kPa
Q_e	Electron charge	C
R	Universal gas constant	J/K mol
r_i	Born radius	m
$r_{i,I}$	Number of segment specie i in component I	
T	Temperature	K
X	Effective local mole fraction	

x	Mole fraction in the liquid phase
Y	Charge composition fraction in local interactions
z	Charge number

Greek letters

α	Non-randomness factor
γ	Activity coefficient
ε	Dielectric constant
μ	Chemical potential
ρ	“Closest approach” parameter
τ	Energy interaction parameter
φ	Fugacity coefficient

Subscript and superscripts

a	Anionic segement specie index
C	Cationic specie index
Born	Born equation
ex	Excess energy
I	Component
I	Component specie index
id	Ideal solution
k	Specie index
L	Liquid phase
lc	Local range contribution
m	Molecular segments specie index
PDH	Long range contribution represented by the Pitzer-Debye-Hückel equation

V	Vapour phase
s	Solvent
w	Water
∞	Infinite dilution
o	Standard state
*	Unsymmetric reference state
⋆	Pure component

Abbreviation

eNRTL	electrolyte Non-Random Two Liquid
FCCU	Fluid catalytic cracking unit
FGD	Flue gas desulphurization
VLE	Vapour-liquid equilibrium

Chapter 1

Introduction

1.1 Background

Sulphur dioxide (SO_2) is a well-known air pollutant due to its harmful effect on human health and on the environment miles away from the emission source. When humans are exposed to high concentration of SO_2, health concerns are breathing difficulties, respiratory illness and aggravation of existing cardiovascular diseases [1]. Concerning the environment, SO_2 is the primary contributor to acid rain causing acidification of lakes and damage on soil and vegetation [2].

The leading source of SO_2 in the air is caused by power plants where SO_2 is formed as a by-product when fossil fuels, particularly coal, are burned. Fossil fuels are the dominant energy source in the world. For instance, in 2012 fossil fuels accounted for 86% of the global primary energy supply [3]. As the energy consumption is assumed to increase, due to increased economic growth, the reliance of fossil fuels is assumed to increase accordingly. However, this unsustainable path of growth is met by increasingly stringent emission regulations, causing well-designed capture technologies to be a necessity.

The most widely adopted method to control SO_2 emission is by using flue gas desulphurization (FGD) technologies, such as the limestone process. The limestone process is the most frequently used FGD technology as it is well-developed and produces saleable gypsum. However, large amount of waste is generated if the supply of gypsum outgrows the demand. Other types of FGD technologies are regenerable processes where the sorbent is regenerated, and sulphur is recovered. The sulphur can be further processed to elemental sulphur, sulphuric acid or liquefied sulphur dioxide. These processes are little applied in the industry, but would be a potential technology to use where there is a demand for sulphur[4]. The largest coal producer and consumer, accounting for 45.6% of the world's coal production, is China [3]. As they also are the world's largest importer of sulphur, a potential FGD technology

that will reduce emission of SO_2 and China's heavy reliance on sulphur imports, is the Labsorb process. Here, SO_2 is captured by a sodium-phosphate-water solution and recovered as a pure SO_2 stream. As mentioned above regenerable processes are little applied, but with regard to the Labsorb process, it exists at least one industrial plant that has installed the processes in full scale. That is the Sannazzoro Refinery operated by ENI in Italy [5]. The reason the process is not more applied is probably due to relatively high investment and operating costs. However, limited information about the process is available in the literature from the refinery in Italy, pilot scale tests and from laboratory studies.

1.2 Scope of the Thesis

As little is known about the Labsorb process, the intended purpose of the thesis is to find an eNRTL thermodynamic model in Aspen Plus that is able to represent the experimental VLE data of the sodium-phosphate-water-SO_2-system. The model is then used to study absorption of SO_2 and to identify energy efficient operating conditions when regenerating SO_2 in the Labsorb process.

1.3 The Labsorb Process

The Labsorb process is a regenerable FGD process used to remove SO_2 from flue gas of a fossil fuel power plant. Sulphur dioxide is recovered and can be further processed to elemental sulphur, sulphuric acid or liquefied sulphur dioxide.

1.3.1 Development History

The Labsorb process was originally invented at Norwegian University of Science and Technology (NTNU) in Trondheim in 1980s as a result of laboratory studies, supervised by Prof. Olav Erga. These promising results were confirmed using a synthetic gas in a skid-mounted pilot-plant at NTNU. Marked by Elkem Technology and under the name the Elsorb process, the results were further confirmed on flue gas from a coal fired boiler at Vitkovice Steel Works in Ostrava, Czech Republic. The pilot test program used a SO_2 load of 3000ppmv [6]. In 1993, ESSO Norway at Slagentangen became the first refinery to install the Elsorb process. The plant treated the off-gas from a Claus tail gas incinerator containing 9800ppmv SO_2 [6].

Today, the Elsorb process goes under the name the Labsorb process and the worldwide exclusive right to mark this technology is with Belco Technologies Corporation, N.J., USA. The Labsorb process is installed at Sannazzorro Refinery operated by ENI in Italy, which process 10 million tons/year of crude oil. The flue gas coming from the fluid catalytic cracking unit (FCCU) contains 1700 mg SO_2/Nm^3 [5].

1.3.2 Process Description

A simplified process flow diagram of the Labsorb process, as applied at the Sannazzoro Refinery, is presented in Figure 1.1.

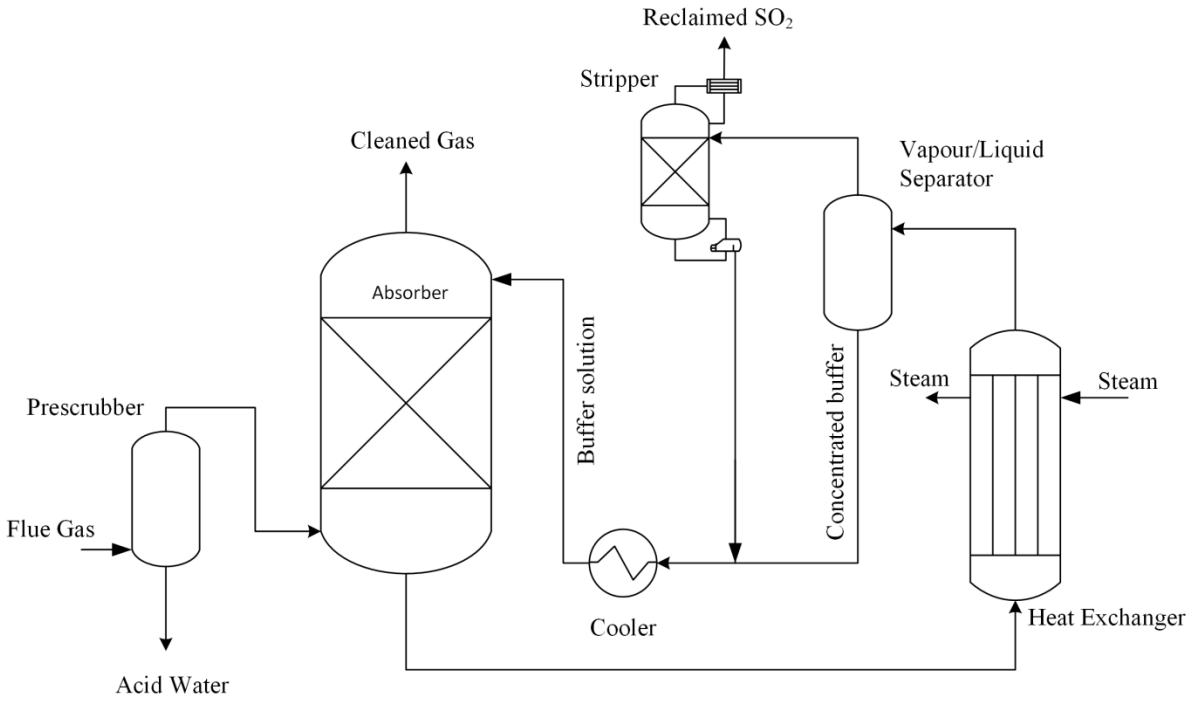

Figure 1.1: Process flow diagram of the Labsorb Process [4].

Here, the incoming SO_2 loaded flue gas is first passed through a pre-scrubber. In the pre-scrubber the flue-gas is cooled to adiabatic saturation temperature, typically around 40 °C to 75 °C, and particulate and acid components such as HF, HCl and SO_3 is removed [7]. Then, the flue gas is led to the absorber where gaseous SO_2 is absorbed into an aqueous sodium-phosphate solution consisting of sodium hydrogen phosphate (Na_2HPO_4,), sodium dihydrogen phosphate (NaH_2PO_4) and sodium sulphate (Na_2SO_4). SO_2 is captured in the form of sodium bisulphite ($NaHSO_3$) and sodium sulphite (Na_2SO_3), while Na_2HPO_4 is simultaneously transformed to NaH_2PO_4. The reactions, summarized below, are instantaneous and reversible within a pH range of 4.5 and 6.5 [8].

SO_2 is dissolved into the aqueous buffer:	$SO_2(g) = SO_2(l)$	1.1
Formation of HSO_3^-:	$SO_2 + 2H_2O = H_3O^+ + HSO_3^-$	1.2
Formation of SO_3^{2-}	$HSO_3^- + OH^- = H_2O + SO_3^{2-}$	1.3
Buffer reaction:	$HPO_4^{2-} + H_3O^+ = H_2PO_4^- + H_2O$	1.4

Due to presence of oxygen in the flue gas, it is expected some precipitation of Na_2SO_4 in the absorber. However, this is counteracted, as will be addressed in the section 1.3.3.

After the absorber, the SO_2 rich buffer solution enters the heat exchanger where steam is used as a heating medium. Here, reactions 1.1-1.4 are reversed such that absorbed SO_2 and water is released from the buffer solution. The buffer solution becomes saturated with respect to Na_2HPO_4 such that crystals containing Na_2HPO_4 may precipitate.

From the heat exchanger, evaporated water vapour and SO_2 is separated from the concentrated buffer solution in a gas/liquid separator and led to a stripper. In the stripper, concentrated SO_2, saturated with water exit the top and is ready for further treatment, while the condensed water is returned to the concentrated buffer solution. The resulting lean buffer solution is cooled to adiabatic saturation temperature and fed back to the absorber. Any potential solids that have formed, is removed from the lean buffer solution before entering the absorber. A bleed of sodium sulphate and sodium phosphate may be necessary in order to maintain the buffer capacity.

1.3.3 Advantages and Disadvantages

The main advantage of the Labsorb process is that it has low oxidation loss. Oxidation studies have reported that the oxidation rate is less than 0.5% of the amount SO_2 being absorbed [9]. The reason for the low oxidation rate is due to the high salting-out effect on O_2 in the flue gas. The salting-out effect states that the solubility of gases, nonpolar solutes and non-ionic solutes are nearly always found to decrease when the salt concentration increases [10]. Therefore, the high concentration of buffer salt in the Labsorb process will ensure low solubility of O_2 in the flue gas such that precipitation of Na_2SO_4 in the absorber is kept low. Furthermore, troublesome incrustation is said to be avoided due to the low daily production ofsolids [8]. The Sannazzoro Refinery operated by ENI in Italy has reported that the daily production of solids consisting of sulphates and phosphates, is 219 kg and 231 kg, respectively [5].

Despite the advantages of the Labsorb process, the process is very little applied. One of the reasons may be high investment and operating cost.

1.4 Outline of the Thesis

The thesis starts with a literature review in chapter 2, followed by a theoretical overview in chapter 3. In the theoretical overview criteria for the vapour-liquid equilibrium (VLE) are derived and the electrolyte Non-Random Two Liquid (eNRTL) activity coefficient model is described.

In chapter 4, the vapour-liquid equilibrium (VLE) of the sodium-phosphate-water-SO_2-system is simulated in ASPEN Plus. First, VLE simulated by the eNRTL model provided by ASPEN Plus is compared to experimental VLE data. Then, two approaches are tested to improve the model's representation of experimental data. The two modified models are compared and one of the models is chosen to be further used in the next chapter, along with the eNRTL model provided by ASPEN Plus.

As a result of the study in chapter 4, one of the modified models and the eNRTL model provided by ASPEN Plus is used when process simulations are conducted in chapter 5. Here, absorption and regeneration of SO_2 are studied and discussed separately.

Main results and recommendations for further work are given in chapter 6.

ASPEN Plus simulation models and Matlab routines, used in this work, are available by request to magne.hillestad@nt.ntnu.no.

Chapter 2

Literature Review

In the 1980s, laboratory studies were conducted at NTNU to measure vapour-liquid equilibria of the sodium phosphate-water-SO_2-system in the temperature range 30 ^{0}C to 70 ^{0}C. These promising results lead to the development of the Labsorb process. This chapter aims to identify and review available information on the Labsorb process and available literature from the VLE studies. Based on the VLE studies, the sodium-phosphate-water-SO_2-system is studied and a solvent to use when simulating the Labsorb process is selected. At the end of the chapter, relevant density data and solid-liquid solubility data in aqueous solution is presented.

2.1 The Labsorb Process

A description of the Labsorb process is given in several published articles [6-8, 11, 12].The Sannazzaro Refinery in Italy, operated by ENI, which have installed the Labsorb Process, has also published an article about the process [5]. In these published articles, process flow diagrams, reactions, unit descriptions, absorption temperature, SO_2 content in the flue gas and SO_2 removal efficiency is presented. In addition, steam requirements when evaporating SO_2 from the buffer solution is reported to be around 11g/gSO_2 [8]. Unfortunately, these published articles do not provide SO_2 concentration in the lean and rich buffer solution, composition or flow rate of the buffer solution, the SO_2 desorption temperature or the boiling point of the buffer solution. Thus, it will be difficult to verify the simulated work. However, an unpublished in-house paper (NTNU) state that the boiling point at atmospheric pressure of the buffer solution is 107 °C, and that the regeneration is assumed to be conducted close to this temperature. For operating conditions of the absorber, collected operating data can be found in a paper presented at the conference “Sulphur 2002” in Vienna (2002) [9]. The operating conditions are presented in Table 2.1.

Table 2.1: Operating conditions in the absorber

Process parameter	Value	Unit
Feed gas flow, wet gas	1000	kNm^3/hr
Absorption temperature	55	°C
Total pressure	1	bara
Superficial gas velocity	3.4	m/s
Tower diameter	11.2	m
SO_2 partial pressure, flue gas	0.003	bar
SO_2 partial pressure, clean gas	0.00017	bar
Absorption efficiency	95	%
Amount of SO_2 Absorbed	127	$kmol_{SO2}/hr$
SO_2 concentration, lean buffer	0.5	$kmol/m^3$
SO_2 concentration, rich buffer	1.6	$kmol/m^3$
Feed rate lean buffer	115	m^3/hr
Corresponding liquid load	1.17	m^3/m^2
Number of packed sections	3	
Packing height	2	m
Packed height per stage	0.3	m

Two remarks can be made of the above table. Firstly, the tabulated feed gas flow of 1000 kNm^3/hr seems to be rounded. Secondly, hand calculations performed to calculate the amount of SO_2 absorbed deviates 0.4% from the tabulated value, 127 kmol/hr. The hand calculations are shown in Appendix A. It seems that all values in Table 2.1 are rounded numbers and it can be questioned whether the numbers are real process data, hand calculations or results from process modelling.

2.2 Vapour- Liquid Equilibrium Studies

The documented work from the vapour-liquid equilibrium (VLE) studies is available in the published article Erga (1988)[8], an internal report[13] and unpublished in-house papers. These papers provide a description of analytical method and experimental execution, but unfortunately, the description is incomplete which makes it difficult to use the VLE data. Data which is missing are, among others; composition of the buffer solution, total pressure, water

vapour pressure, density of unloaded and loaded solution and the uncertainty of the experimental results.

In this work, the VLE data are taken from Hove (2013) [14]. The VLE data are presented in Table 2.2 to Table 2.5 for the buffer solutions 2.5/1.25/0.5, 2.5/0.83/0.5, 2.5/0.25/0.5 and 3/1/0.5, respectively. When the notation buffer 3/1/0.5 is used, it denotes that the buffer composition is $C_{Na_2HPO_4}$ = 3 mol/L, $C_{NaH_2PO_4}$ = 1 mol/L and $C_{Na_2SO_4}$ = 0.5 mol/L.

Table 2.2: Experimental vapour-liquid equilibrium data for buffer 2.5/1.25/0.5

T=40 °C		**T=55 °C**		**T=70 °C**	
C_{SO2} [mol/L]	**P_{SO2} [ppm]**	**C_{SO2} [mol/L]**	**P_{SO2} [ppm]**	**C_{SO2} [mol/L]**	**P_{SO2} [ppm]**
0.41	$2.45*10^{-5}$	0.41	$4.60*10^{-5}$	0.41	$8.20*10^{-5}$
0.50	$4.30*10^{-5}$	0.50	$8.30*10^{-5}$	0.50	$1.53*10^{-4}$
0.60	$7.80*10^{-5}$	0.60	$1.54*10^{-4}$	0.60	$2.85*10^{-4}$
0.70	$1.36*10^{-4}$	0.70	$2.68*10^{-4}$	0.70	$5.00*10^{-4}$
0.80	$2.20*10^{-4}$	0.80	$4.30*10^{-4}$	0.80	$8.40*10^{-4}$
0.90	$3.40*10^{-4}$	0.90	$6.60*10^{-4}$	0.90	$1.31*10^{-3}$
1.00	$5.20*10^{-4}$	1.00	$1.00*10^{-3}$	1.00	$1.98*10^{-3}$
1.10	$7.60*10^{-4}$	1.10	$1.45*10^{-3}$	1.10	$2.85*10^{-3}$
1.20	$1.08*10^{-3}$	1.20	$2.10*10^{-3}$	1.20	$4.00*10^{-3}$
1.30	$1.50*10^{-3}$	1.30	$2.90*10^{-3}$	1.30	$5.50*10^{-3}$
1.34	$1.70*10^{-3}$	1.34	$3.30*10^{-3}$	1.34	$6.20*10^{-3}$

Table 2.3: Experimental vapour-liquid equilibrium data for buffer 2.5/0.83/0.5

T=40 °C		T=55 °C		T=70 °C	
C_{SO2} [mol/L]	P_{SO2} [ppm]	C_{SO2} [mol/L]	P_{SO2} [ppm]	C_{SO2} [mol/L]	P_{SO2} [ppm]
0.50	$2.00*10^{-5}$	0.40	$1.85*10^{-5}$	0.40	$3.30*10^{-5}$
0.60	$3.90*10^{-5}$	0.50	$4.20*10^{-5}$	0.50	$7.00*10^{-5}$
0.70	$7.00*10^{-5}$	0.60	$8.00*10^{-5}$	0.60	$1.35*10^{-4}$
0.80	$1.20*10^{-4}$	0.70	$1.40*10^{-4}$	0.70	$2.45*10^{-4}$
0.90	$1.90*10^{-4}$	0.80	$2.40*10^{-4}$	0.80	$4.20*10^{-4}$
1.00	$3.00*10^{-4}$	0.90	$3.80*10^{-4}$	0.90	$6.80*10^{-4}$
1.10	$4.50*10^{-4}$	1.00	$5.80*10^{-4}$	1.00	$1.04*10^{-3}$
1.20	$6.60*10^{-4}$	1.10	$8.60*10^{-4}$	1.10	$1.54*10^{-3}$
1.30	$9.50*10^{-4}$	1.20	$1.23*10^{-3}$	1.20	$2.20*10^{-3}$
1.40	$1.31*10^{-3}$	1.30	$1.73*10^{-3}$	1.30	$3.10*10^{-3}$
1.50	$1.81*10^{-3}$	1.40	$2.40*10^{-3}$	1.40	$4.20*10^{-3}$
		1.50	$3.20*10^{-3}$		

Table 2.4: Experimental vapour-liquid equilibrium data for buffer 2.5/0.25/0.5

T=40 °C		T=55 °C		T=70 °C	
C_{SO2} [mol/L]	P_{SO2} [ppm]	CSO2 [mol/L]	P_{SO2} [ppm]	C_{SO2} [mol/L]	P_{SO2} [ppm]
0.70	$2.90*10^{-5}$	0.53	$1.70*10^{-5}$	0.53	$2.70*10^{-5}$
0.80	$5.10*10^{-5}$	0.60	$2.90*10^{-5}$	0.60	$4.60*10^{-5}$
0.90	$8.50*10^{-5}$	0.70	$5.60*10^{-5}$	0.70	$9.80*10^{-5}$
1.00	$1.35*10^{-4}$	0.80	$1.00*10^{-5}$	0.80	$1.84*10^{-4}$
1.10	$2.10*10^{-4}$	0.90	$1.70*10^{-4}$	0.90	$3.20*10^{-4}$
1.20	$3.20*10^{-4}$	1.00	$2.75*10^{-4}$	1.00	$5.35*10^{-4}$
1.30	$4.60*10^{-4}$	1.10	$4.20*10^{-4}$	1.10	$8.60*10^{-4}$
1.40	$6.60*10^{-4}$	1.20	$6.40*10^{-4}$	1.20	$1.30*10^{-3}$
1.50	$9.50*10^{-4}$	1.30	$9.20*10^{-4}$	1.30	$1.90*10^{-3}$
1.59	$1.27*10^{-3}$	1.40	$1.31*10^{-4}$	1.40	$2.70*10^{-3}$
		1.50	$1.82*10^{-3}$	1.50	$3.75*10^{-3}$
		1.59	$2.45*10^{-3}$	1.59	$4.90*10^{-3}$

Table 2.5: Experimental vapour-liquid equilibrium data for buffer 3/1/0.5

T=30 °C		T=40 °C		T=55 °C		T=70 °C	
C_{SO2} [mol/L]	P_{SO2} [ppm]	C_{SO2} [mol/L]	P_{SO2} [ppm]	C_{SO2} [mol/L]	P_{SO2} [ppm]	C_{SO2} [mol/L]	P_{SO2} [ppm]
1.16	$1.65*10^{-4}$	0.65	$4.35*10^{-5}$	0.52	$4.11*10^{-5}$	0.57	$7.82*10^{-5}$
1.38	$3.38*10^{-4}$	0.88	$1.06*10^{-4}$	0.67	$7.93*10^{-5}$	0.79	$2.68*10^{-4}$
1.66	$8.17*10^{-4}$	1.18	$3.05*10^{-4}$	0.98	$2.94*10^{-4}$	0.98	$4.9*10^{-4}$
1.69	$1.06*10^{-3}$	1.47	$7.92*10^{-4}$	1.24	$6.98*10^{-4}$	1.14	$7.76*10^{-4}$
1.96	$2.67*10^{-3}$	1.53	$9.70*10^{-4}$	1.37	$1.00*10^{-3}$	1.34	$1.84*10^{-3}$
2.02	$2.59*10^{-3}$	1.55	$1.04*10^{-3}$	1.45	$1.31*10^{-3}$	1.47	$2.75*10^{-3}$
2.24	$5.46*10^{-3}$	1.72	$1.82*10^{-3}$	1.47	$1.38*10^{-3}$	1.59	$3.97*10^{-3}$
2.58	$1.62*10^{-2}$	1.74	$1.90*10^{-3}$	1.65	$2.09*10^{-3}$	1.86	$7.92*10^{-3}$
		1.75	$1.89*10^{-3}$	1.84	$3.73*10^{-3}$		
		1.92	$2.76*10^{-3}$	1.89	$4.18*10^{-3}$		
		1.94	$2.84*10^{-3}$	2.01	$6.57*10^{-3}$		
		2.08	$4.31*10^{-3}$	2.14	$8.82*10^{-3}$		
		2.12	$6.39*10^{-3}$				
		2.26	$1.08*10^{-2}$				

Here, C_{SO2} is the concentration of absorbed SO_2 and P_{SO2} is the partial pressure of SO_2. In total, it is 142 data points in the concentration range 0.4 mol_{SO2}/L to 2.58 mol_{SO2}/L, and in the temperature range 30 °C to 70 °C.

When examining the above tables, it can be seen that vapour-liquid equilibrium has been studied in a narrow SO_2 concentration range, and only in the temperature range 30 °C to 70 °C. The unit which is used for the four buffer solutions and for the amount of SO_2 absorbed is mole per litre unloaded solution and mole per litre loaded solution, respectively. Unfortunately, mole per litre is a challenging unit, especially when the unloaded and loaded density is unknown. Regarding the partial pressure of SO_2, ppm is used as a unit. As the total pressure is not given it is difficult for an exact conversion from ppm to the unit atmospheric pressure or Pascal. Further, the temperature, which the buffer solutions were characterized at, is also not given.

Finally, when studying the values for the SO_2 concentration, tabulated in Table 2.2 to

Table 2.4, for buffer solution 2.5/1.25/0.5, 2.5/0.83/0.5 and 2.5/0.25/0.5, respectively, it can be seen that the exact same amount of SO_2 has been added (0.1 mol_{SO2}/L) to each measurement. As it is unknown how the solutions were prepared, it is not known how it was possible to always have the same addition of SO_2.

2.3 The Sodium-Phosphate-Water-SO_2-System

From VLE data, given in the section above, one can examine how the concentration of Na_2HPO_4 and NaH_2PO_4 affects absorption of SO_2. The equilibrium reactions occurring in the liquid phase of the sodium phosphate-water-SO_2-system are as given in equation 1.2 to 1.4. In Figure 2.1, VLE data for buffer solution 2.5/1.25/0.5, 2.5/0.83/0.5, 2.5/0.25/0.5 and 3/1/0.5 at 55 ˚C is presented.

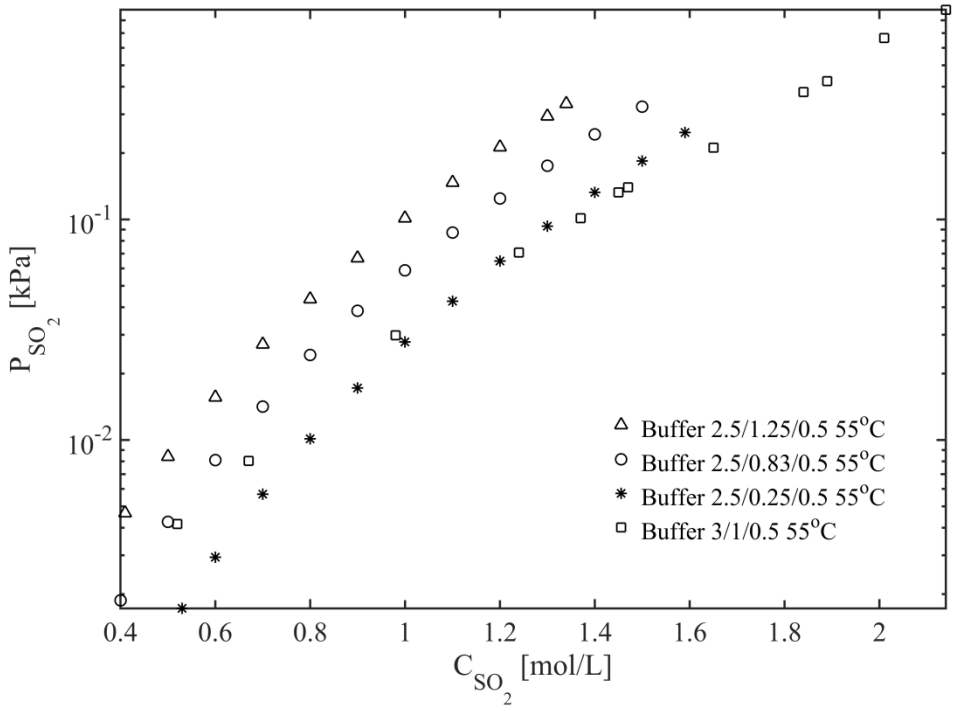

Figure 2.1: Experimental VLE data for buffer 2.5/1.25/0.5, 2.5/0.83/0.5, 2.5/0.25/0.5 and 3/1/0.5 at 55 °C

Here, one can see that when the concentration of NaH_2PO4 is decreasing from 1.25 $mol_{NaH2PO4}$/L to 0.25 $mol_{NaH2PO4}$/L, the partial pressure of SO_2 is decreasing. Lower SO_2 partial pressure indicates higher absorption capacity and the increase in absorption can be explained by the change in pH. Since NaH_2PO4 is more acidic than Na_2HPO_4, NaH_2PO_4 will lower the pH, while Na_2HPO_4 will increase the pH. When the solution becomes more basic

the equilibrium of HSO_3^- shifts to favour SO_3^{2-} which then allows higher SO_2 absorption to be achieved. From Figure 2.1 it can also be seen that buffer 3/1/0.5 has quite similar SO_2 partial pressure as buffer 2.5/0.25/0.5. It seems that when the concentration of Na_2HPO_4 and NaH_2PO_4 is increased from 2.5 $mol_{Na2HPO4}$/L to 3.0 $mol_{Na2HPO4}$/L and 0.25 $mol_{NaH2Po4}$/L to 1.0 $mol_{NaH2Po4}$/L, respectively, there is almost no change in pH.

2.4 Selection of Solvent

As identified in section 2.1, it is not known which buffer solution that is used in the Labsorb process. As there are no significant differences between the solvents at 55°C, shown in Figure 2.1, and VLE data above 70°C is not available, it is not easy to select a suitable solvent. However, in this work buffer 3/1/0.5 is selected as solvent. Buffer 3/1/0.5 is the solvent with most experimental data and is regarded as a relevant solvent [15]. This buffer solution will be used when absorption and regeneration of SO_2 is simulated in ASPEN Plus.

2.5 Density and Solid-Liquid Solubility Data

Experimental density and solid-liquid solubility data for the sodium-phosphate-water-SO_2-system is not found in the literature. However, density and solid-liquid solubility data for the components: Na_2HPO_4, NaH_2PO_4 and Na_2SO_4, in aqueous solution can be found in the literature.

In the literature, the density data of aqueous solution refer to a temperature of 20 °C and is given as a function of concentration (moles of solute per litre of solution). Density data of Na_2HPO_4, NaH_2PO_4 and Na_2SO_4 is found in the concentration range 0.035-0.369 $mol_{Na2HPO4}$/L, 0.408-4.499 $mol_{NaH2PO4}$/L and 0.035-1.875 mol_{Na2SO4}/L, respectively [16]. In the literature, solid-liquid solubility data for the components, and their hydrated form, in aqueous solution can be found in the temperature range 0 °C to 100 °C as shown in Figure 2.2 [17, 18].

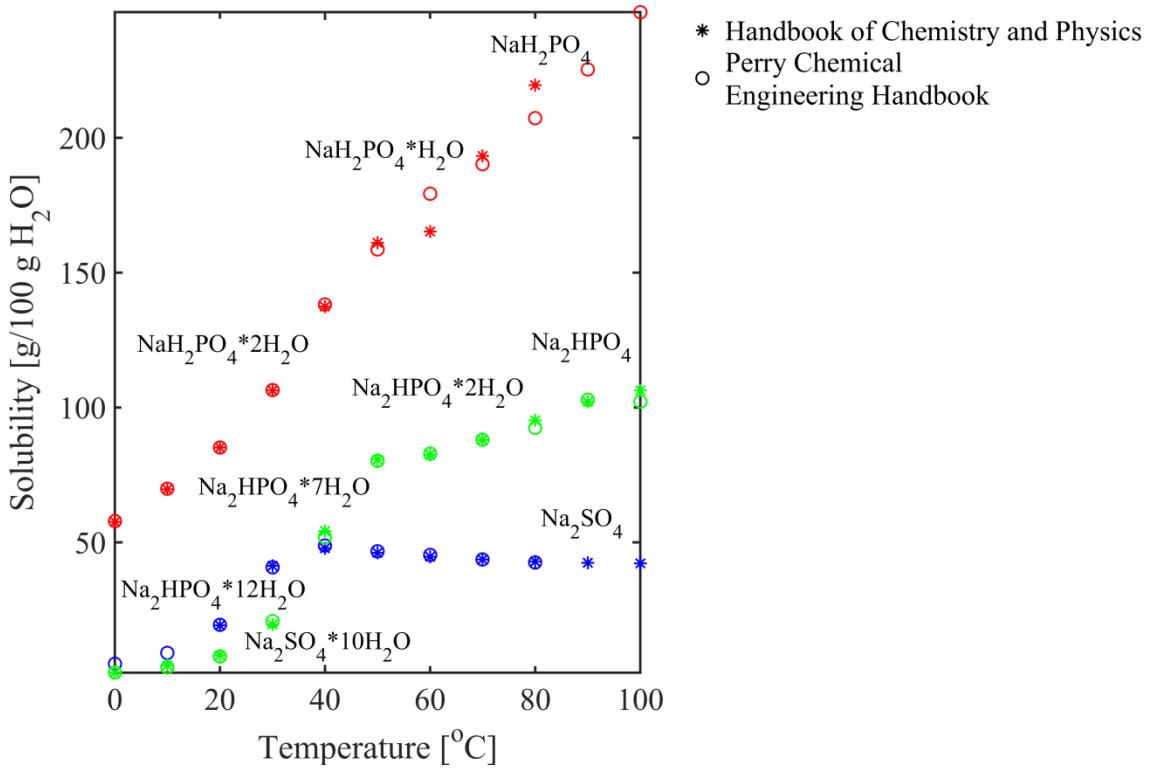

Figure 2.2: Solid-liquid solubility of Na_2HPO_4, NaH_2PO_4 and Na_2SO_4, and their hydrated form, in aqueous solution.

2.6 Conclusion

To summarize, operating conditions of the Labsorb process are not well reported. The analytical and experimental method from VLE studies is only partly explained and there are no experimental data above 70 °C. Consequently, it will be difficult to use the VLE data and verify simulations. Buffer 3/1/0.5 was selected as solvent and will be used when simulating the Labsorb process.

Chapter 3

Theoretical Framework

During absorption and regeneration of SO_2, vapour and liquid phases are brought into contact. When the phases are not at equilibrium, mass transfer occur between the phases. Vapour-liquid equilibrium (VLE) plays a decisive role when designing the Labsorb process and can be regarded as the heart of the process. In this chapter, criteria for VLE are derived and the eNRTL activity coefficient model, used in ASPEN Plus, is described.

3.1 Vapour Liquid Phase Equilibrium

Vapour-liquid equilibrium (VLE), is a condition where no macroscopic changes occurs in the vapour or in the liquid phase [19]. This implies that the phase composition, temperature and pressure reach final values which thereafter remain constant. Although there are no changes between the phases, the concentration of a component in the vapour and liquid phase is often different from each other. The difference is due to departure from ideal behaviour which can be described by Raoult's and Henrys law. Raoult's law, given in equation 3.1, states that the partial vapour pressure of component i in an ideal mixture, P_i, is equal to the product of mole fraction of component i in the liquid-phase, x_i, and the vapour pressure of pure component i, $P_i^\star$, at temperature T [20].

$$P_i = P_i^\star x_i \tag{3.1}$$

Henry's law, given in equation 3.2, says that the amount of a gas which can dissolve in a liquid, at a specific temperature, is proportional to the gas partial pressure over the liquid [20]. Here, H is henrys constant.

$$P_i = H x_i \tag{3.2}$$

The equilibrium condition for the vapour and liquid phase can be derived on the basis of the Gibbs energy. The total differential Gibbs energy, G, is written as follows:

$$dG = \left(\frac{\partial G}{\partial T}\right)_{P,\mathrm{n}_i} dT + \left(\frac{\partial G}{\partial P}\right)_{\mathrm{T},\mathrm{n}_i} dP + \sum_i \left(\frac{\partial G}{\partial n_i}\right)_{\mathrm{T,P,n}_{j\neq i}} dn_i \qquad 3.3$$

Here, n_i is the number of mole of the specie i and the summation is over all present species where the subscript $n_{j\neq i}$ indicates that species other than i are held constant. Further, the partial derivative of the Gibbs energy with respect to the number of moles of specie i is defined as the chemical potential, μ, as follows.

$$\mu_i \equiv \left(\frac{\partial G}{\partial n_i}\right)_{\mathrm{T,P,n}_{j\neq i}} \qquad 3.4$$

When considering a vapour and a liquid phase in a closed system at equilibrium, the temperature and pressure in the two phases will be the same and uniform throughout the system and Gibbs energy is minimised, i.e. $(dG)_{T,P} = 0$ [19, 21]. Therefore, at equilibrium equation 3.3 is reduced to:

$$(dG)_{T,P,n} = \sum_i \mu_i^V dn_i^V + \sum_i \mu_i^L dn_i^L = 0 \qquad 3.5$$

Here, the subscript V and L denotes vapour and liquid phase, respectively. The changes between dn_i^V and dn_i^L is caused by mass transfer between the phases, and as mass is conserved [19] it is required that

$$-dn_i^V = dn_i^L \qquad 3.6$$

Therefore,

$$\sum_i \left(\mu_i^V - \mu_i^L\right) dn_i^L = 0 \qquad 3.7$$

As dn_i^L is an independent and arbitrary value [19], equation 3.7 can only be zero if

$$\mu_i^V = \mu_i^L \qquad \text{i=1,2,3…N} \qquad 3.8$$

Here, N is the number of species. The equilibrium condition in equation 3.8 can be further generalised to multiple phases where it exists α, β…ω equilibrium phases

$$\mu_i^\alpha = \mu_i^\beta = \cdots = \mu_i^\omega \qquad \text{i=1,2,3…N} \qquad 3.9$$

Thus, the vapour and liquid phase, at the same temperature and pressure, are in equilibrium when the chemical potential of each species is the same in all phases. Equation 3.9 denotes the fundamental criterion for phase and chemical equilibrium, but it is seldom used directly as chemical potential is highly inconvenient to use. However, G.N Lewis (1901) [22] developed a new quantity called fugacity f_i. When fugacity of component i in a mixture with constant temperature is defined as [19]:

$$d\mu_i = RTd\ln f_i \qquad 3.10$$

Then the vapour and liquid phase equilibrium can be written as

$$\mu_i^V - \mu_i^L = RT\ln\frac{f_i^V}{f_i^L} = 0 \rightarrow f_i^V = f_i^L \qquad 3.11$$

Consequently, fugacity can be used as a working criterion of equilibrium. The fugacity can be related to the fugacity coefficient, φ, and the activity coefficient, γ_i, which both is a measure of non-ideality.

The fugacity is related to the dimensionless fugacity coefficient as follows

$$f = \varphi P \qquad 3.12$$

where the fugacity coefficient is a function of temperature and pressure and can be calculated from an equation of state (EOS) [21].

The fugacity is related to the activity coefficient as follows.

$$\gamma_i = \frac{a_i}{x_i} = \frac{f_i}{f_i^0} \qquad 3.13$$

Here, f_i^0 is the standard fugacity coefficient and a_i is the activity. The activity coefficient is further related to the composition through the partial derivative of the excess Gibbs energy, G^{ex}, with respect to the change in mole of specie i as follows:

$$\ln \gamma_i = \frac{1}{RT}\left(\frac{\partial G^{\text{ex}}}{\partial n_i}\right)_{T,P,n_{j\neq i}} \qquad 3.14$$

The excess Gibbs energy, G^{ex}, is defined as given in equation 3.15,

$$G^{ex} = G - G^{id} \qquad 3.15$$

Here, G is the Gibbs energy of a solution and G^{id} is the Gibbs energy of an ideal solution at the same temperature, pressure and composition.

Moreover, the general equation when vapour and liquid phase equilibrium is established is as follows [21]

$$\varphi_i y_i P = \gamma_i x_i \varphi_i^{sat} \, \mathrm{P}_i^{sat} \exp\left(\frac{v_i^L (P - P_i^{sat})}{RT}\right) \qquad 3.16$$

Here, φ_i and γ_i are the gas phase fugacity and liquid phase activity coefficient for component i, respectively, φ_i^{sat}, is the fugacity coefficient for saturated vapour and the exponential term is the pointing factor which accounts for the compressibility effects within the liquid [19].

3.2 Electrolyte Non-Random Two Liquid (NRTL) Activity Coefficient Model

Several activity coefficient models have been developed by different researchers [23-29]. In this work, the electrolyte Non-Random Two Liquid (eNRTL) activity coefficient model is of interest as it is widely used for aqueous multicomponent electrolyte systems. The eNRTL

activity coefficient model is built into the eNRTL thermodynamic model, provided by the chemical process modelling software ASPEN Plus version 8.6.

The electrolyte NRTL activity coefficient model assumes that the deviation from ideality is caused by long-range and local-range interactions, and that these contributing terms are additive [30]. The long-range interactions are represented by the Pitzer-Debye-Hückel (PDH) model and the Born equation, and the local-range interactions are represented by the Non-random Two Liquid (NRTL) theory. When these terms are added together, as given in equation 3.17, the general fundamental expression for the excess Gibbs energy in the eNRTL thermodynamic model is obtained [31].

$$G_m^{*\mathrm{ex}} = G_m^{*\mathrm{ex,PDH}} + G_m^{*\mathrm{ex},Born} + G_m^{*\mathrm{ex},lc} \qquad 3.17$$

Here, $G_m^{*\mathrm{ex}}$ is the excess Gibbs energy in an electrolyte system, $G_m^{*\mathrm{ex,PDH}}$ and $G_m^{*\mathrm{ex},Born}$ is the contribution from the long-range interactions and $G_m^{*\mathrm{ex},lc}$ is the contribution from the local-range interaction. The notation "*" denotes the unsymmetric reference state which, in this work, is chosen to be the infinite dilute aqueous solution, that is $\gamma_i^* \to 1 \text{ as } x_{H_2O} \to 1$. When applying equation 3.14 on equation 3.17, the expression for the activity coefficient of electrolyte systems is obtained:

$$\ln \gamma_I^* = \ln \gamma_I^{*\mathrm{PDH}} + \ln \gamma_I^{*\mathrm{Born}} + \ln \gamma_I^{*\mathrm{lc}} \qquad 3.18$$

Details for the long-range and local-range interactions are given in the sections below.

3.2.1 NRTL Term for Long-Range Interaction Contribution

The long-range interaction contribution is represented by the Pitzer-Debye-Hückel model and the Born equation.

The Pitzer-Debye-Hückel model

The Long-range interaction between ionic species is represented by the unsymmetric Pitzer-Debye-Hückel formula as follows [31]:

$$\ln \gamma_i^{*PDH} = -\left(\frac{1000}{M_s}\right)^{1/2} A_\varphi \left[\left(\frac{2z_i^2}{\rho}\right)\ln\left(1+\rho I_X^{1/2}\right)+\frac{z_i^2 I_X^{1/2}-2I_X^{1/2}}{1+\rho I_X^{1/2}}\right] \quad 3.19$$

With:

$$A_\varphi = \frac{1}{3}\left(\frac{2\pi N_A d_S}{1000}\right)^{1/2}\left(\frac{Q_e^2}{\varepsilon_S k_B T}\right)^{1/2} \quad 3.20$$

$$I_X = \frac{1}{2}\sum_i x_i z_i^2 \quad 3.21$$

Here A_φ is the Debye-Hückel parameter, I_X is the ionic strength, M_s is the molecular weight of the solvent s and ρ is the "closest approach" parameter. Further, N_A is Avogadro's number, d_s is the density of the solvent s, Q_e is the electron charge, ε_s is the dielectric constant of the solvent s, k_B is the Boltzmann constant and z_i is the charge number of ion i.

For a component I consisting of solvent molecular segments, m, cationic segments, c, and anionic segments, a, the logarithm of the activity coefficient is the sum of the various segments contributions as follows [30]

$$\ln \gamma_I^{*\mathrm{PDH}} = \sum_m r_{m,I} \ln \gamma_m^{*\mathrm{PDH}} + \sum_c r_{c,I} \ln \gamma_c^{*\mathrm{PDH}} + \sum_a r_{a,I} \ln \gamma_a^{*\mathrm{PDH}} \quad 3.22$$

Here, $r_{m,I}$, $r_{c,I}$ and $r_{a,I}$ are number of molecular, cationic and anionic segment species in component I, respectively.

The born equation

The unsymmetric reference state in the Pitzer-Debye-Hückel formula is defined as mixed-solvent solution at the infinite-dilution. However, the desired reference state is aqueous solution at infinite-dilution [30]. Therefore, in order to correct the change of reference state from the mixed-solvent solution to the aqueous solution, the Born equation must be applied:

$$\ln \gamma_i^{*Born} = \frac{Q_e^2}{2k_B T}\left(\frac{1}{\varepsilon_S}-\frac{1}{\varepsilon_W}\right)\frac{z_i^2}{r_i}10^{-2} \qquad i = c,\ a \quad 3.23$$

Here ε_w is the dielectric constant of water and r_i is the born radius of specie i which can be a cation c, or an anion a.

For a component I, the logarithm of the activity coefficient is the sum of the various segments contributions:

$$\ln \gamma_I^{*\text{Born}} = \sum_c r_{\text{c},I} \ln \gamma_c^{*Born} + \sum_a r_{\text{a},I} \ln \gamma_a^{*\text{Born}} \qquad 3.24$$

3.2.2 NRTL Term for Local-Range Interaction Contribution

The local-range interaction contribution is represented by the NRTL model proposed by Chen et. al (1982)[29]. The basic assumption behind the NRTL approach is that the nonideal entropy of mixing is negligible compared to the heat of mixing. Since electrolyte systems are characterized with extremely large heat of mixing, is this assumption consistent [29].

There are two fundamental assumptions in the NRTL model which are applied when considering an electrolyte system [31]:

1. *The like-ion repulsion assumption*: Repulsive forces between ions of same charge is so strong that the composition of anions around anions is zero (and likewise for cations).

2. *The local electroneutrality assumption:* The net charge is zero when cations and anions are distributed around a central molecule.

In a simple electrolyte system all species can be categorized into three species: molecular species, m, cationic species, c and anionic species, a. Further, it is assumed that there are three types of local composition interactions in the mixing as illustrated in Figure 3.1 [31].

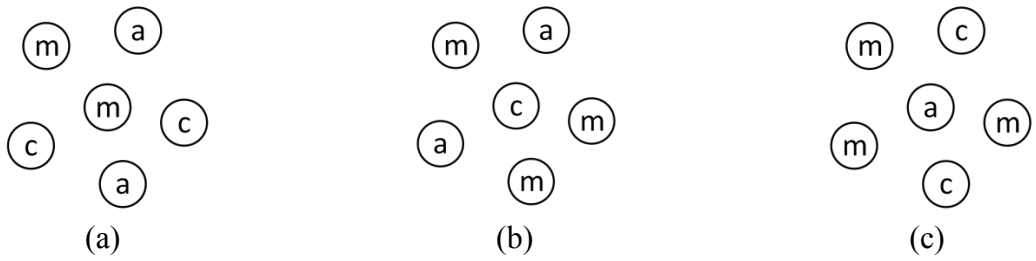

Figure 3.1: (a) Solvent molecule at centre, (b) cation at centre, (c) anion at centre

Type (a) consists of a central molecule surrounded by molecules, cations and anions. Here the local electroneutrality assumption is applied. Type (b) consists of a central cation surrounded by molecules and anions, and type (c) consists of a central anion surrounded by solvent molecules and cations. Both (b) and (c) are based on the like-ion repulsion assumption.

Accordingly, the logarithm of the activity coefficient of local-range interactions for molecular components, cations and anions can be written as equation 3.25, 3.26 and 3.27, respectively [30].

$$\ln \gamma_m^{lc,I} = \frac{\sum_j X_{j,I} G_{jm} \tau_{jm}}{\sum_k X_{\mathrm{k},I} G_{km}} + \sum_{m'} \frac{X_{m',I} G_{mm'}}{X_{\mathrm{k},I} G_{km'}} \left(\tau_{mm'} - \frac{\sum_k X_{\mathrm{k},I} G_{km'} \tau_{km'}}{\sum_k X_{\mathrm{k},I} G_{km'}} \right) + \sum_c \sum_a \frac{Y_a X_{c,I} G_{mc,ac}}{\sum_k X_{k,I} G_{kc,ac}} \left(\tau_{mc,ac} - \frac{\sum_k X_{\mathrm{k},I} G_{kc,ac} \tau_{kc,ac}}{\sum_k X_{\mathrm{k},I} G_{kc,ac}} \right) + \sum_a \sum_c \frac{Y_c X_{\mathrm{a},I} G_{ma,\mathrm{ca}}}{\sum_k X_{k,I} G_{ka,ca}} \left(\tau_{mc,ca} - \frac{\sum_k X_{\mathrm{k},I} G_{ka,\mathrm{ca}} \tau_{ka,ca}}{\sum_k X_{\mathrm{k},I} G_{ka,\mathrm{ca}}} \right) \qquad \mathrm{k = m, c, a} \qquad 3.25$$

$$\frac{1}{z_c} \ln \gamma_c^{lc,I} = \sum_a Y_a \frac{\sum_k X_{\mathrm{k},I} G_{kc,ac} \tau_{kc,ac}}{\sum_k X_{\mathrm{k},I} G_{kc,ac}} + \sum_m \frac{X_{m,I} G_{cm}}{\sum_k X_{\mathrm{k},I} G_{km}} \left(\tau_{cm} - \frac{\sum_k X_{\mathrm{k},I} G_{km} \tau_{km}}{\sum_k X_{\mathrm{k},I} G_{km}} \right) + \sum_a \sum_c \frac{Y_{c'} X_{\mathrm{a},I} G_{ca,\mathrm{c'a}}}{\sum_k X_{k,I} G_{ka,c'a}} \left(\tau_{ca,c'a} - \frac{\sum_k X_{\mathrm{k},I} G_{ka,\mathrm{c'a}} \tau_{ka,c'a}}{\sum_k X_{\mathrm{k},I} G_{ka,\mathrm{c'a}}} \right) \qquad \mathrm{k = m, c, a} \qquad 3.26$$

$$\frac{1}{z_a} \ln \gamma_a^{lc,I} = \sum_c Y_c \frac{\sum_k X_{\mathrm{k},I} G_{ka,ca} \tau_{ka,ca}}{\sum_k X_{\mathrm{k},I} G_{ka,ca}} + \sum_m \frac{X_{m,I} G_{am}}{\sum_k X_{\mathrm{k},I} G_{km}} \left(\tau_{am} - \frac{\sum_k X_{\mathrm{k},I} G_{km} \tau_{km}}{\sum_k X_{\mathrm{k},I} G_{km}} \right) + \sum_c \sum_{a'} \frac{Y_{a'} X_{\mathrm{c},I} G_{ac,\mathrm{a'c}}}{\sum_k X_{k,I} G_{ac,\mathrm{a'c}}} \left(\tau_{ac,\mathrm{a'c}} - \frac{\sum_k X_{\mathrm{k},I} G_{ka,\mathrm{a'c}} \tau_{ka,\mathrm{a'c}}}{\sum_k X_{\mathrm{k},I} G_{kc,\mathrm{a'c}}} \right) \qquad \mathrm{k = m, c, a} \qquad 3.27$$

With

$$G_{ji} = \exp(-\alpha_{ji} \tau_{ji}) \qquad \mathrm{i,j = m, c, a} \qquad 3.28$$

$$X_{j,I} = C_j x_{j,I} \qquad \mathrm{j = m, c, a} \qquad 3.29$$

Here, k denotes the species index, X is the effective local mole fraction, C_j equals the charge

number for ionic species and 1 for molecular species, x_j is the segment based mole fraction of specie i, and Ya and Yc is the anionic and cationic charge composition fraction quantity, respectively. Further is α_{ji} the non-randomness factor, which is inherently symmetric and τ_{ji} is the energy interaction parameter.

For a component I, the logarithm of the activity coefficient of local-range interactions is the sum of the various segments contribution:

$$\ln \gamma_I^{\mathrm{lc}} = \sum_m r_{\mathrm{m},I} \ln \gamma_m^{\mathrm{lc}} + \sum_c r_{\mathrm{c},I} \ln \gamma_c^{\mathrm{lc}} + \sum_a r_{\mathrm{a},I} \ln \gamma_a^{\mathrm{lc}} \qquad 3.30$$

Equation 3.30 has a symmetric reference state, but can be corrected to an unsymmetric reference state as follows [30]:

$$\begin{aligned} \ln \gamma_I^{*\mathrm{lc}} &= \ln \gamma_I^{lc} - \ln \gamma_I^{\infty lc} \qquad \text{i = m, c, a} \qquad 3.31 \\ &= \sum_i r_{i,I} (\ln \gamma_i^{lc} - \ln \gamma_i^{\infty lc}) \end{aligned}$$

Here, $\ln \gamma_i^{\infty lc}$ is the infinite-dilute activity coefficient in aqueous solution and can be obtained from the following equations below.

$$\ln \gamma_m^{\infty lc} = \tau_{wm} + G_{mw}\tau_{mw} \qquad 3.32$$

$$\frac{1}{z_c} \ln \gamma_c^{\infty lc} = \sum_a Y_a \tau_{wc,ac} + G_{cw}\tau_{cw} \qquad 3.33$$

$$\frac{1}{z_a} \ln \gamma_a^{\infty lc} = \sum_c Y_a \tau_{wa,ca} + G_{aw}\tau_{aw} \qquad 3.34$$

The notation w is water.

3.2.3 Main Adjustable Parameter in the NRTL Model

The main adjustable parameter in the NRTL activity coefficient model is the binary interaction energy parameter, τ, for local range interactions [31]. The parameter is found in equation 3.25 to 3.27 and is associated with the binary molecule-molecule pairs, electrolyte-molecule pairs and electrolyte-electrolyte pairs. In the context of the electrolyte NRTL model, molecules are molecular solvent species and dipolar species, and electrolytes are cation-anion

pairs [32]. Since binary interaction energy parameters are asymmetric there are two binary interaction energy parameters per binary pair. The temperature dependence relationship of the binary interaction energy parameters are as follows:

Molecule-molecule binary interaction energy parameters:

$$\tau_{mm'} = A_{mm'} + \frac{B_{mm'}}{T} + F_{mm'} \ln(T) + G_{mm'} T \tag{3.35}$$

$$\tau_{m'm} = A_{m'm} + \frac{B_{m'm}}{T} + F_{m'm} \ln(T) + G_{m'm} T \tag{3.36}$$

Electrolyte-molecule binary interaction energy parameters:

$$\tau_{ca,m} = C_{ca,m} + \frac{D_{ca,m}}{T} + E_{ca,m}\left[\frac{Tref - T}{T} + \ln\left(\frac{T}{Tref}\right)\right] \tag{3.37}$$

$$\tau_{m,ca} = C_{m,ca} + \frac{D_{m,ca}}{T} + E_{m,ca}\left[\frac{Tref - T}{T} + \ln\left(\frac{T}{Tref}\right)\right] \tag{3.38}$$

Electrolyte-electrolyte binary interaction energy parameters:

$$\tau_{c'a,c''a} = C_{c'a,c''a} + \frac{D_{c'a,c''a}}{T} + E_{c'a,c''a}\left[\frac{Tref - T}{T} + \ln\left(\frac{T}{Tref}\right)\right] \tag{3.39}$$

$$\tau_{ca',ca''} = C_{ca',ca''} + \frac{D_{ca',ca''}}{T} + E_{ca',ca''}\left[\frac{Tref - T}{T} + \ln\left(\frac{T}{Tref}\right)\right] \tag{3.40}$$

Here, A, B, C, D, E, F and G are binary parameters, m is solvent molecule, ca is cation-anion electrolyte pair and T_{ref} = 298.15 K. The binary parameters can be retrieved from the built-in eNRTL binary databank in ASPEN Plus or be determined through regression of VLE data [31]. The names of the binary parameters in ASPEN Plus v8.6 is given below.

Table 3.1: The name of the molecule-molecule binary parameters in ASPEN Plus

Parameter	Parameter ASPEN Plus
$A_{mm'}$, $A_{m'm}$	NRTL/1
$B_{mm'}$, $B_{m'm}$	NRTL/2
$F_{mm'}$, $F_{m'm}$	NRTL/5
$G_{mm'}$, $G_{m'm}$	NRTL/6

Table 3.2: The name of the electrolyte-molecule binary parameters in ASPEN Plus

Parameter	Parameter ASPEN Plus
$C_{ca,m}$, $C_{m,ca}$	GMELCC
$D_{ca,m}$, $D_{m,ca}$	GMELCD
$E_{ca,m}$, $E_{m,ca}$	GMELCE

Table 3.3: The name of the electrolyte-electrolyte binary parameters in ASPEN Plus

Parameter	Parameter ASPEN Plus
$C_{c'a,c''a}$,$C_{ca'',ca'}$	GMELCC
$D_{c'a,c''a}$, $D_{ca'',ca'}$	GMELCD
$E_{c'a,c''a}$, $E_{ca'',ca'}$	GMELCE

Chapter 4

Simulation of Vapour-Liquid Equilibrium

For an accurate simulation of the Labsorb process, it is essential that the simulation tool has a proper representation of the experimental VLE data in the sodium-phosphate-water-SO_2 system. As discussed earlier in this work, the sodium-phosphate-water-SO_2-system is simulated in ASPEN Plus v8.6 using the eNRTL model. The eNRTL model applies the activity coefficient model, described in section 3.3, to account for the non-ideal liquid behaviour in aqueous and mixed-solvent electrolyte systems. Redlich-Kwong equation of state is used to describe the behaviour of real gases. The aim of the chapter is to find an eNRTL model that is able to represent the experimental VLE data, and which can be used to simulate the Labsorb process. First, VLE is simulated in the eNRTL model provided by ASPEN Plus. Then, due to lack of experimental data for temperatures above 70 °C, artificial VLE data are generated using a simple VLE model (soft model). Thereafter, two attempts to fit binary parameters in the eNRTL model are presented and the models are compared with the eNRTL model provided by ASPEN Plus.

4.1 Simulation of VLE in the Standard Model

To investigate VLE in ASPEN Plus, the eNRTL model provided by ASPEN Plus, hereafter called the *standard model*, is used. Here, the chemistry and relevant parameters are automatically created using the "elec-wizard" button. The binary interaction parameters of the *standard model* are given in Appendix D.

When experimental VLE data from buffer 3/1/0.5, given in Table 2.5, are compared with values from ASPEN Plus, it can be seen from Figure 4.1 that ASPEN Plus over-predicts the SO_2 partial pressure at SO_2 concentrations below 1.3mol_{SO2}/L in the temperature range 40°C to 70 °C.

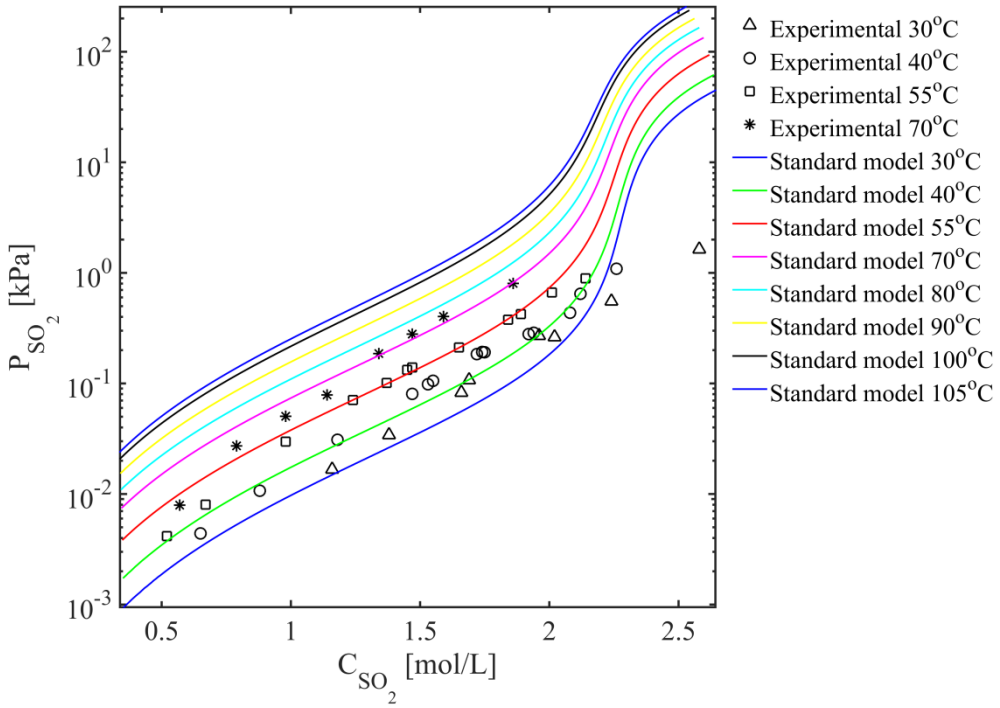

Figure 4.1: The partial pressure of SO_2 as a function of the SO_2 concentration in the aqueous phosphate buffer solution 3/1/05. The average deviation of the *standard model* is 37.9%.

Here, the average deviation is 37.9%, when the very highest concentration, 2.58 mol_{SO2}/L at 30 °C, is not included. The average deviation is calculated from the equations below.

$$\%\text{Error} = \left| \frac{P_{\text{exp},i} - P_{cal,i}}{P_{\text{exp},i}} \right| 100\% \qquad 4.1$$

$$\%\text{Average deviation} = \sum_{i=1}^{n} \frac{\%Error}{N} \qquad 4.2$$

For temperatures above 70 °C the VLE curves are behaving reasonable, but as addressed in the literature review, there has not been conducted experimental VLE studies above 70 °C. It is therefore not possible to validate these curves with experimental data.

The VLE-curves where buffer 2.5/1.25/0.5, 2.5/0.83/0.5 and 2.5/0.25/0.5 is compared with experimental data is given in Appendix B. Here, the average deviation is 40.4%, 41.7% and 37.3%, respectively.

In order to improve the *standard model* representation of experimental VLE data, binary parameters in the eNRTL model were fitted to VLE data. As there are no experimental data above 70 °C, an attempt was made to use a simple soft model to generate artificial VLE data at higher temperatures to improve the results of parameter fitting in ASPEN Plus.

4.2 Artificial VLE Data

To generate artificial VLE data for the sodium-phosphate-water-SO_2-system for temperatures above 70 °C, a "soft model" was used [33]. The function is given in equation 4.3 and relates SO_2 partial pressure, $P_{SO2,}$ with loading, α (mol_{SO2}/mol_{Na+}).

$$\ln p_{SO_2} = A\ln\alpha + k_1 + \frac{B}{1 + k_2 \exp(-k_3 \ln\alpha)} \qquad 4.3$$

Here, A, B, k_1,k_2 and k_3 are parameters and all k_i parameters are linear functions of the inverse temperature. It should be emphasized that the function is only a parameterized fit and has no thermodynamic significance. Additionally, VLE data generated from a simple empirical model can never replace experimental data as a truly reliable source of data.

The soft model function is incorporated into a Matlab routine written by Hertzberg et. al.(1998) [33] and the experimental data from buffer 2.5/1.25/0.5, 2.5/0.83/0.5, 2.5/0.25/0.5 and 3/1/0.5 given in Table 2.2 to Table 2.5, respectively, were used for the fitting. For each buffer solution a set of parameters to implement into equation 4.3 was found and artificial partial pressures of SO_2 were generated in the temperature range 30 °C to 105 °C. In Table 4.1 the parameters for buffer 3/1/0.5 are presented, and in Figure 4.2 the artificial VLE data are compared with experimental data. VLE data generated in the temperature range 80 °C to 105 °C are also included in Figure 4.2

Table 4.1: Parameters for buffer 3/1/0.5 used in the soft model function

Parameter	Value
A	4.46
B	6.04
k_1	-4363.38*(1/T) + 18.96
k_2	exp(-150993.24*(1/T) - 501.43)
k_3	-117986.51*(1/T) + 393.63

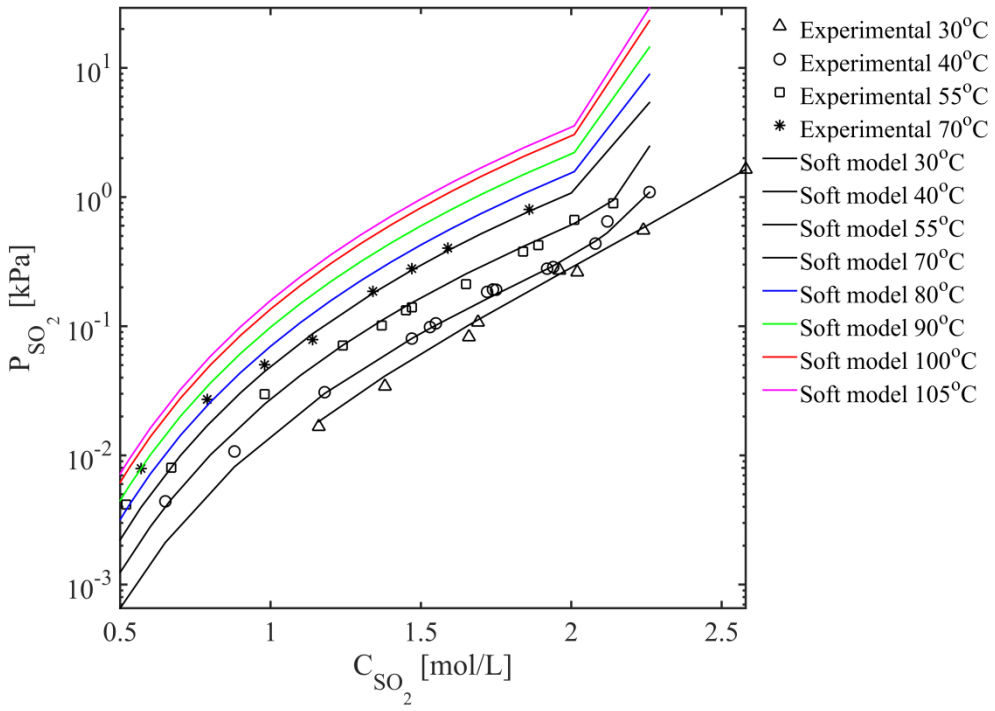

Figure 4.2: The partial pressure of SO_2 as a function of the SO_2 concentration in the aqueous phosphate buffer solution 3/1/0.5.The average deviation of the soft model is 13.2%

In Figure 4.2, the VLE data generated by the soft model were fitted to the experimental data with an average deviation of 13.2%. It can be seen that the soft model is able to predict the partial pressure of SO_2 well at high SO_2 concentrations, while at SO_2 concentrations below 1.0 mol_{SO2}/L the partial pressure of SO_2 is under-predicted. The tendency to under-predict may be a result of few experimental points at low loadings. As a consequence, it is reason to believe that SO_2 partial pressures generated in the temperature range 80 °C to 105 °C is also under-predicted at SO_2 concentrations below 1.0 mol_{SO2}/L.

The parameters and the artificial VLE data compared with experimental data from buffer 2.5/1.25/0.5, 2.5/0.83/0.5 and 2.5/0.25/0.5 is presented in Appendix C. Here, the partial pressure values are predicted well, but as for buffer 3/1/0.5, they have a small tendency to under-predict the partial pressure of SO_2 at low SO_2 concentrations.

4.3 Fitting of the Standard Model in ASPEN Plus

In an attempt to improve the *standard model*s representation of experimental VLE data in the sodium phosphate-water-SO_2-system in ASPEN Plus, the binary parameters in the eNRTL model were fitted to VLE data. The first modified *standard model*, hereafter called *model 1*, used experimental VLE data, given in Table 2.2 to Table 2.5, to fit binary parameters. The second modified *standard model*, hereafter called *model 2*, used experimental VLE data and VLE data generated by the soft model, presented in Figure 4.2 and Appendix C, in the temperature range 80 °C to 105 °C.

4.3.1 Methodology

The *standard model* was modified by fitting binary parameters, for local-range interactions, described in section 3.3, to VLE data. In this work, the binary parameters, A and B, for molecule-molecule interactions, given in equation 3.35 and 3.36, and the binary parameters, C and D, for electrolyte-molecule interactions, given in equation 3.37 and 3.38, were fitted. The molecule-molecule and electrolyte-molecule interaction pairs that were assumed to have the greatest impact on the sodium phosphate-water-SO_2-system were chosen. Overview of the species and binary parameters to be fitted is presented in Table 4.2. In total, 24 binary parameters were fitted.

Table 4.2: The species and binary parameters for the molecule-molecule and molecule-electrolyte interaction pairs.

Interaction pair	Species	Binary parameter
Molecule-molecule	SO_2, H_2O	A,B
Electrolyte-molecule	H_2O, Na^+, $H_2PO_4^-$	C, D
	H_2O, Na^+, HPO_4^{2-}	
	H_2O, Na^+, HSO_3^-	
	H_2O, Na^+, SO_3^{2-}	
	H_2O, Na^+, SO_4^{2-}	

The electrolyte-electrolyte interaction pairs and remaining molecule-molecule and electrolyte-molecule interaction pairs, which were not fitted, were set to zero. The non-randomness factor, α, for molecule-molecule and electrolyte-molecule interactions were fixed at 0.2 as suggested by Chen and Evans (1986) [34].

The binary parameters were fitted to VLE data with the use of an unpublished in-house Matlab routine which connects MATLAB to ASPEN Plus. The fitted binary parameters are given in Appendix D. Before the Matlab routine was run, desired VLE calculations were entered into the generic property analysis in ASPEN Plus. Below follows a description of the steps that were required in the generic property analysis and a short description of the in-house Matlab routine.

The generic property analysis in ASPEN Plus

The generic property analysis is a tool which can perform flash calculations. Here, temperature and vapour fraction was set as constant and property set for the SO_2 partial pressure and the concentration of SO_2, SO_3^{2-} and HSO_3^- were created in order to report a result. Further, the composition of the unloaded buffer solutions; 2.5/1.25/0.5, 2.5/0.83, 2.5/0.25/0 and 3/1/0.5 and the flow of loaded SO_2 were specified. For *model 1* and *2*, 142 and 338 VLE data points were used, respectively, to fit the binary parameters.

To insert the correct buffer composition and mass fraction of SO_2 from VLE data into the generic property analysis was a challenge. As addressed in the literature review, converting to mole or mass becomes problematic when the unit is mol/L and density of loaded and unloaded SO_2 solutions are not known.

The problem was solved by using densities found from ASPEN Plus. It is not known which temperature the solutions were characterized at, but 20 °C was assumed to be a reasonable temperature. The density of buffer solution; 2.5/1.25/0.5, 2.5/0.83, 2.5/0.25/0 and 3/1/0.5 at 20 °C, retrieved from ASPEN Plus, are tabulated in Table 4.3.

Table 4.3: The density of the buffer solutions at 20 °C retrieved from ASPEN Plus

Buffer solution	Density [g/cm^3]
Buffer 2.5/1.25/0.5	1.4923
Buffer 2.5/0.83/0.5	1.4568
Buffer 2.5/0.25/0.5	1.4071
Buffer 3/1/0.5	1.5359

To give an idea whether densities calculated in ASPEN Plus were reasonable, the density of the components; Na_2HPO_4, NaH_2PO_4 and Na_2SO_4 in aqueous solution at a given concentration were compared with values from the literature at 20 °C [16]. The comparison is presented in Table 4.4.

Table 4.4: The density of the components; Na_2HPO_4, NaH_2PO_4 and Na_2SO_4 in aqueous solution at a given concentration at 20°C

Component	mol/L	Density from literature [g/cm3]	Density from ASPEN [g/cm3]
Na_2HPO_4	0,408	1,0528	1,0531
NaH_2PO_4	4,499	1,3493	1,3904
Na_2SO_4	1,875	1,2106	1,2123

Here, it was found that the density of the components Na_2HPO_4, NaH_2PO_4 and Na_2SO_4 in aqueous solution in ASPEN Plus deviated 0.03%, 3.04% and 0.14%, respectively, from the literature data. Due to the small deviations, it was assumed that ASPEN Plus is also able to calculate densities of the aqueous phosphate buffer solution quite good.

For the SO_2 equilibrium concentration, the issue became more complex as the density of the SO_2 loaded buffer solution varies with SO_2 loading and temperature. In total, one needed 142 and 338 densities for *model 1* and *2*, respectively, in order to find the desired SO_2 fraction to be entered into the analysis. Since it is time consuming to find that amount of densities, a faster option was to run the generic property analysis with an SO_2 mass fraction range of 0.015 to 0.1 and with an increment of $1.25*10^{-4}$. Thereafter, the desired SO_2 equilibrium concentration was combined with the corresponding mass fraction, which was used as an input in the analysis. When the analysis was run, correct SO_2 concentration was calculated.

When all VLE data had been entered into the generic property analysis, the simulation was reinitialized and ready to be processed by MATLAB.

The in-house Matlab routine

The in-house Matlab routine connects MATLAB to ASPEN Plus. When the routine is run, Matalab sends a set of binary parameters to ASPEN Plus, which then feeds Matlab with calculated SO_2 partial pressures. Once the Matlab routine has processed the partial pressures it sends a new set of binary parameters to ASPEN Plus in order to minimize the difference between the simulated and the experimental SO_2 partial pressure. This sequence is repeated until there are no further improvements after 75 iterations. When the routine has terminated, the ASPEN Plus file contains a new set of binary parameters and the generic property analysis can be run to study simulated VLE.

A known problem with the Matlab routine is that when ASPEN Plus receives a new set of binary parameters such that activity coefficients are changed, the density and the composition in the liquid phase also changes [35]. The change is most evident at high loadings such that the initial SO_2 concentration at high SO_2 loadings are not the same after the Matlab routine has terminated. However, as the change in concentration was less than 4.5%, at all temperatures, it was not decisive for the final result.

4.3.2 Simulation of VLE in Model 1 and 2

When fitting of binary parameters were complete, VLE were simulated in *model 1* and *2* in ASPEN Plus, and compared with experimental data. Below is first VLE data compared in the temperature range 30 °C and 70 °C and then in the temperature range 80 °C and 105 °C.

Temperature range 30 °C to 70 °C

The ability of *model 1* and *2* to predict experimental SO_2 partial pressure for the buffer solution 3/1/0.5 is presented in Figure 4.3.

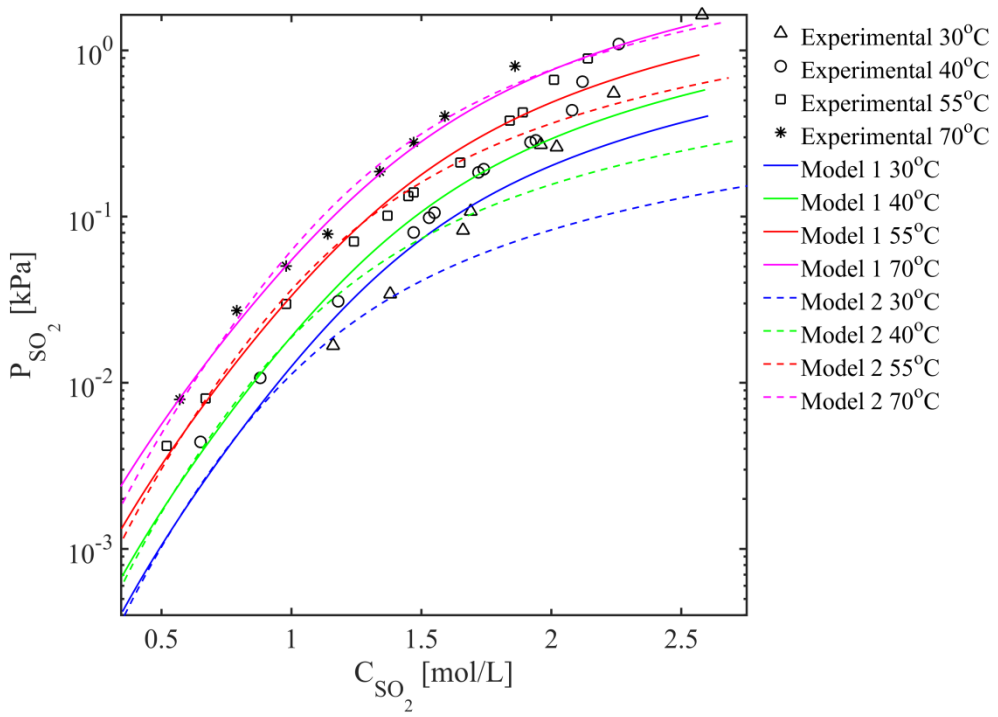

Figure 4.3: The partial pressure of SO_2 as a function of the SO_2 concentration in the aqueous phosphate buffer solution 3/1/05. The average deviation of *model 1* and *2* are 16.8% and 24.4%, respectively.

Here, it can be seen that at 70 °C both models predicts lower SO_2 partial pressure at SO_2 concentrations above 1.6 mol_{SO2}/L. At 55 °C and 40 °C, *model 1* under-predict the SO_2 partial pressure at SO_2 concentrations above 1.9 mol_{SO2}/L and 1.8 mol_{SO2}/L, respectively, while *model 2* under-predict the SO_2 partial pressure at SO_2 concentrations above 1.7 mol_{SO2}/L and 1.5 mol_{SO2}/L, respectively. The reason for the under-prediction could be the small amount of data at SO_2 concentrations above 1.6 mol_{SO2}/L: buffer 3/1/0.5 is the only buffer solution which covers SO_2 concentrations above 1.6 mol_{SO2}/L. When the spread of data is poor, the fitting of binary parameters may fail to find good binary parameters to predict the partial pressure of SO_2 at a wide range of liquid concentrations of SO_2. Another explanation could be the choice of fitted binary parameters. Since, it is not found literature of a similar fitting of the sodium-phosphate-water-SO_2-system, the amount of binary parameters and which binary parameters to fit were selected based on the components which were believed to have the greatest impact on the system. At 30 °C, both of the models are generally unable to predict the SO_2 partial pressure. This poor prediction is again most likely due to few experimental data as VLE data at 30 °C is only present for buffer 3/1/0.5. One option which could have solved the

issue with few and poorly spread experimental data would have been to also use VLE data, in the temperature range 30 °C to 70 °C, generated by the soft model discussed in section 4.2.

In Figure 4.3, *model 1* has an average deviation of 16.8% and thereby the lowest deviation compared to *model 2* having a deviation of 24.4%. *Model 1* is able to represent the experimental VLE data in the temperature range 40 °C to 70 °C in the SO_2 concentration range 0.5 mol_{SO2}/L to 1.6 mol_{SO2}/L. This range covers the relevant temperatures and SO_2 concentrations in the process simulations.

In Appendix E, the VLE curves for buffer 2.5/1.25/0.5, 2.5/0.83 and 2.5/0.25/0.5 at 40°C, 55 °C and 70 °C is presented. Here, the average deviation of *model 1* and *2* is 9.2% and 10%, respectively, for buffer 2.5/0.83/0.5, and 18.5% and 21.4%, respectively, for buffer 2.5/0.25/0.5. Concerning buffer 2.5/1.25/0.5, both of the models are under predicting the SO_2 partial pressure at SO_2 concentrations above 0.6 mol_{SO2}/L. The reason why some of the buffer solutions have a better representation of the experimental VLE data is not known, especially not as nearly the same amount of experimental data, and in the same SO_2 concentration range, has been used for all of the three buffer solutions.

When comparing the VLE-curves, discussed above, it is observed that the average deviation is always higher for *model 2*. Therefore, it is noticed that when VLE data at low and high temperatures is used to fit binary parameters, they will affect each other. If VLE data at high temperatures is incorrect it will most likely have a negative effect on the prediction of partial pressure at low temperatures.

Temperature range 80°C to 105 °C

The ability of *model 2* to predict the high temperature VLE data generated by the soft model for buffer 3/1/0.5 is presented in Figure 4.4

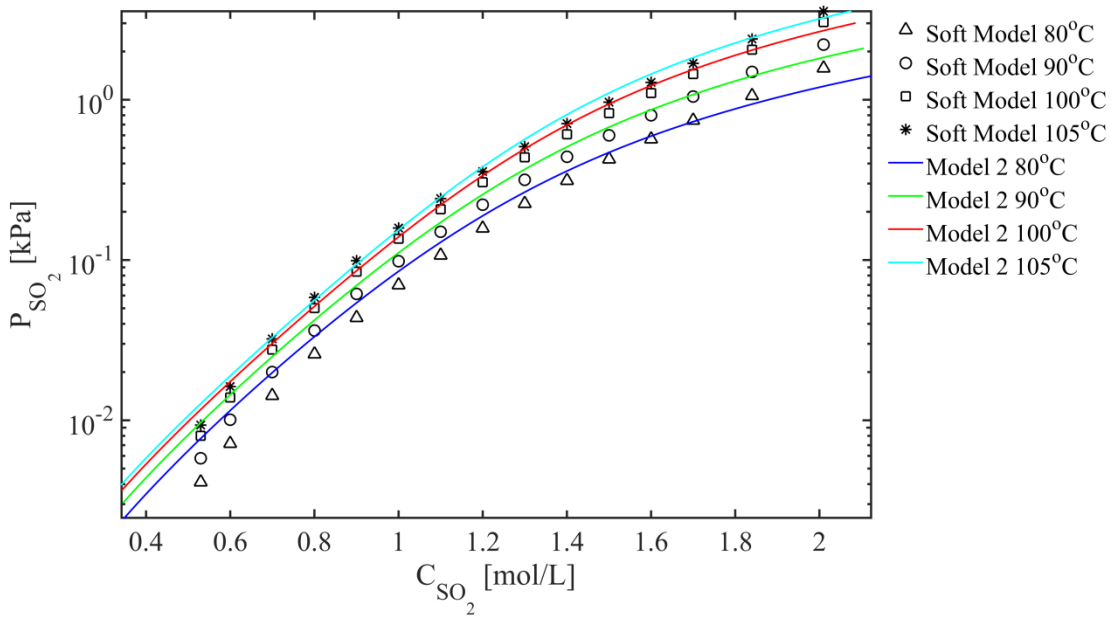

Figure 4.4: The partial pressure of SO_2 as a function of the SO_2 concentration in the aqueous phosphate buffer solution 3/1/05. The average deviation of *model 2* is 17.0%.

Here, *model 2* predicts the partial pressure of SO_2 well at SO_2 concentrations higher than 1.0 mol_{SO2}/L. For concentrations below 1.0mol_{SO2}/L, the model has a tendency to over-predict the SO_2 partial pressure. However, this over-prediction might be good as it was found from Figure 4.2 that the SO_2 partial pressure generated by the soft model at SO_2 concentrations below 1.0 mol_{SO2}/L most likely were under-predicted. When studying the VLE curves shown in Appendix E for the remaining buffer solutions, it is clear that *model 2* cannot be used for these buffer solutions since the partial pressure of SO_2 at low SO_2 concentrations are under-predicted within all buffer solutions. *Model 2* is unable to predict the partial pressure of SO_2 for buffer 2.5/1.25/0.5.

In Figure 4.5, *model 1* and *2* is compared in the temperature range 80 °C to 105 °C.

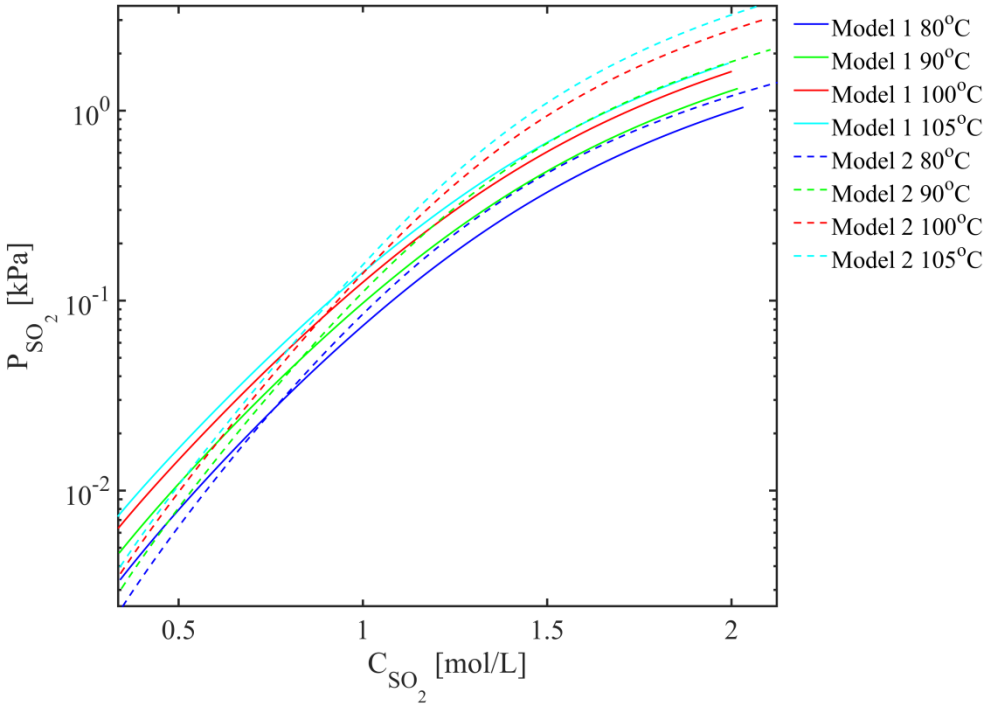

Figure 4.5: The partial pressure of SO_2 as a function of the concentration of SO_2, in the aqueous phosphate buffer solution 3/1/0.5.

From Figure 4.5, it is observed that *model 1* has higher SO_2 partial pressures compared to *model 2* at low SO_2 concentrations, while *model 2* has higher SO_2 partial pressure values at high SO_2 concentrations.

As a result of the discussion above, related to the lower average deviation of *model 1* at low temperatures, *model 1* will be used further in this work.

4.4 Comparing the Standard Model and Model 1

In Figure 4.6 and Figure 4.7, the *standard model* is compared with *model 1* in the temperature range 30 °C to 70 °C and 80 °C to 105 °C, respectively.

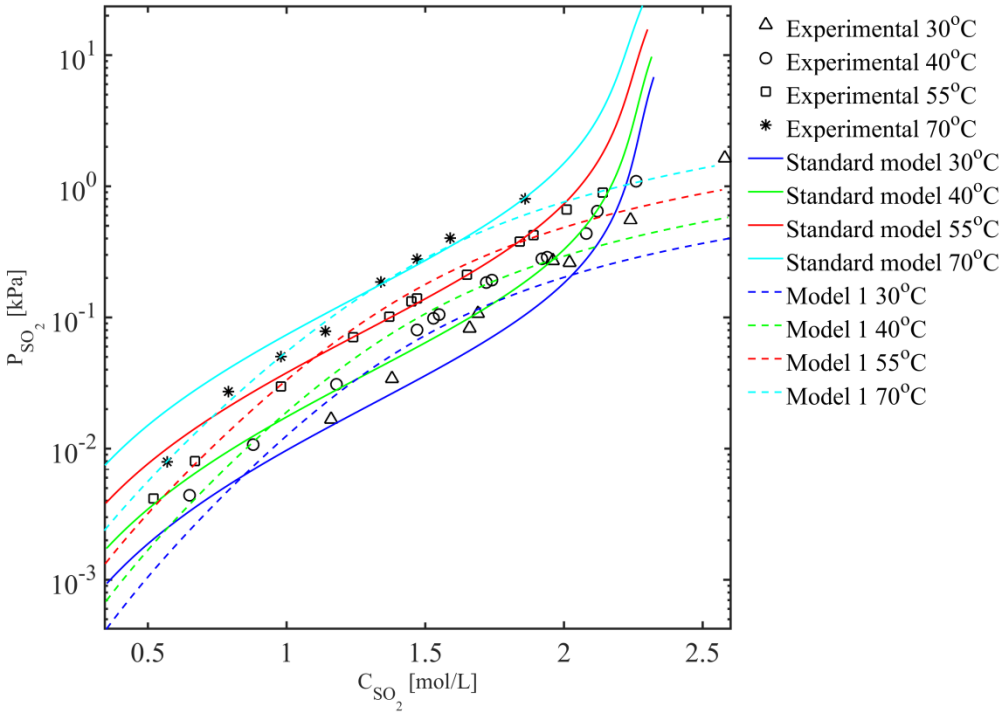

Figure 4.6: The partial pressure of SO_2 as a function of the SO_2 concentration in the aqueous phosphate buffer solution 3/1/05.The average deviation of the *standard model* and *model 1* is 37.9% and 16.8%, respectively

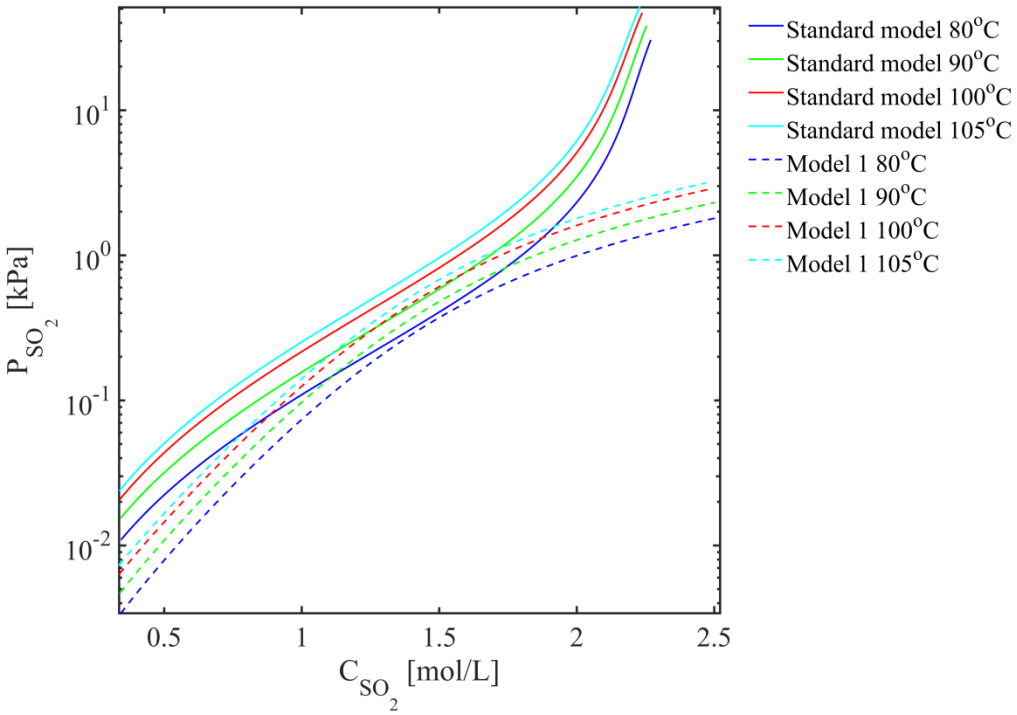

Figure 4.7: The partial pressure of SO_2 as a function of the SO_2 concentration in the aqueous phosphate buffer solution 3/1/05.

As seen from Figure 4.6 *model 1* is able to predict the experimental SO_2 partial pressure better compared the *standard model* in the temperature range 30 °C to 70 ^{o}C. To be more specific; the average deviation for buffer 3/1/0.5 has been improved from 37.9% to 16.8%. Thus, taking into account the small amount of experimental data as discussed earlier, it is clear that the method used to improve VLE in ASPEN Plus works.

In Figure 4.7, the *standard model* has higher partial pressure values at all temperatures up to 105 °C. The difference in the predictions is large and will greatly influence the simulation results. For example, as listed in Table 2.1 the SO_2 concentration at the absorber inlet is given to be 0.5 mol_{SO2}/L. At this SO_2 loading, the partial pressure of SO_2 in the *standard model* and *model 1* is 0.05 kPa and 0.01 kPa, respectively. Consequently, the *standard model* has a SO_2 partial pressure which is 5 times higher compared to *model 1*.

Furthermore, from the two figures it can be seen that model 1 is more temperature sensitive at both high and low temperatures compared to the standard model. For illustration, when the SO_2 loading is 0.5 mol_{SO2}/L and the temperature is increased from 80 °C to 105 °C, the SO_2 partial pressure is increased from 0.023 kPa to 0.052 kPa in the *standard model* and 0.0079 kPa to 0.0082 kPa in *model 1*. Thus, the SO_2 partial pressure increases a factor of 2.26 in the *standard model* while only a factor of 1.03 in *model 1*. The difference in SO_2 partial pressure, mentioned above, and in temperature sensitivity will cause dissimilarities when regeneration of SO_2 is simulated. Regeneration of SO_2 will be discussed in section 5.2.

From the two figures it is also clear that the fitting of binary parameters in ASPEN Plus have a big influence on the behaviour of the vapour-liquid equilibrium curve. In both of the figures, it can be seen that the partial pressure of SO_2, in the *standard model*, is increasing rapidly at SO_2 concentrations around 1.8 mol_{SO2}/L, while in *model 1* this rapid increase of partial pressure is not present.

Chapter 5

Simulation of Absorption and Regeneration of SO_2

From the literature review, it is clear that there is limited information available concerning operating conditions of the Labsorb process. Therefore, the main goal of this chapter is to study absorption of SO_2 in the sodium-phosphate-water-SO_2-system and to find energy efficient operating conditions for regeneration of SO_2. Absorption and regeneration of SO_2 are simulated separately in ASPEN Plus, using the *standard model* and *model 1* discussed in the previous chapter. Both, the absorption and regeneration section is simulated using operating conditions, given in Table 2.1, as a starting point.

5.1 Absorption of SO_2

Absorption of SO_2 was simulated by using the equilibrium-based RadFrac column in ASPEN Plus. An equilibrium-based model approach considers liquid and vapour stream, leaving a stage, to be at equilibrium and an efficiency factor accounts for the deviation from equilibrium. In this work, the efficiency factor was set to 1 as kinetics of the system were unknown. When kinetics of the system is unknown rate-based model approach cannot be considered.

Absorption of SO_2 was studied at three different temperatures; 45 °C, 55 °C and 65 °C. The concentration of SO_2 in the gas phase, 3000 ppm and the SO_2 concentration in the buffer solution entering the top stage of the absorber, 0.5 mol_{SO2}/L, were chosen based on Table 2.1. The ASPEN plus simulation model is illustrated in Figure 5.1.

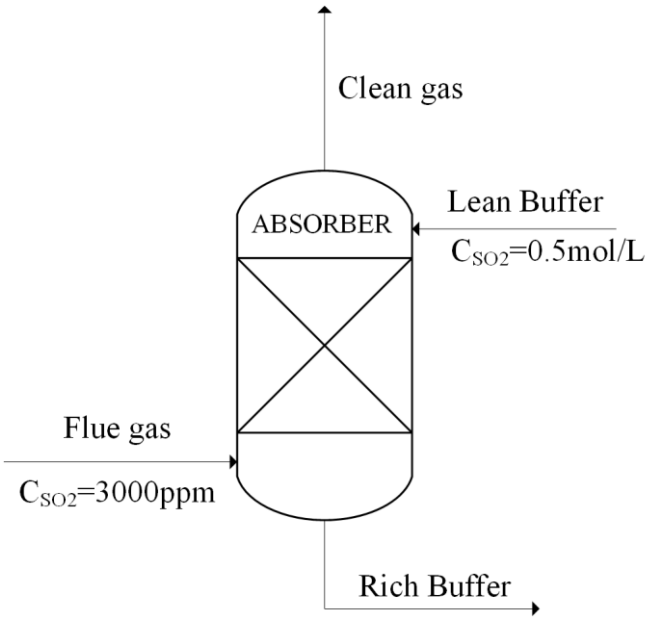

Figure 5.1: Illustration of the absorber simulated in ASPEN Plus.

The flue gas, entering the absorber, is estimated to be a typical flue gas from a coal fired power plant and is saturated with water. The partial pressure of water can be calculated by the Antonio equation[36] given below.

$$\log p_{H_2O}^{sat} = A - \frac{B}{(T+C)} \qquad 5.1$$

Here A, B and C are constants with the values: A=8.07131, B=1730.63 and C=233.426

Thus, the composition and condition of the flue gas is presented in Table 5.1.

Table 5.1: Condition and composition of the flue gas

Parameter	Value	Value	Value
Flow rate [kNm^3/h]	1000	1000	1000
Temperature [°C]	45	55	65
Pressure [bar]	1.01325	1.01325	1.01325
Composition [mole %]			
SO_2	0.3	0.3	0.3
H_2O	9.43	15.49	24.6
CO_2	9.38	9.38	9.38
N_2	76.0	69.96	60.83
O_2	4.85	4.85	4.85

5.1.1 Equilibrium Stages

The first part of the study was to determine the number of equilibrium stages in the absorber column. The number of stages was set so that simulation results were reached without being influenced by number of stages. In Figure 5.2, the SO_2 removal efficiency as a function of the number of stages is plotted. Here, it can be seen that the SO_2 absorption efficiency, in both of the models, stabilizes after around 10 stages and that there are no significant difference between 10 and 14 stages. Thus, in all simulations at least 10 stages are needed. When absorption of SO_2 is studied in the section below, 10 stages are used.

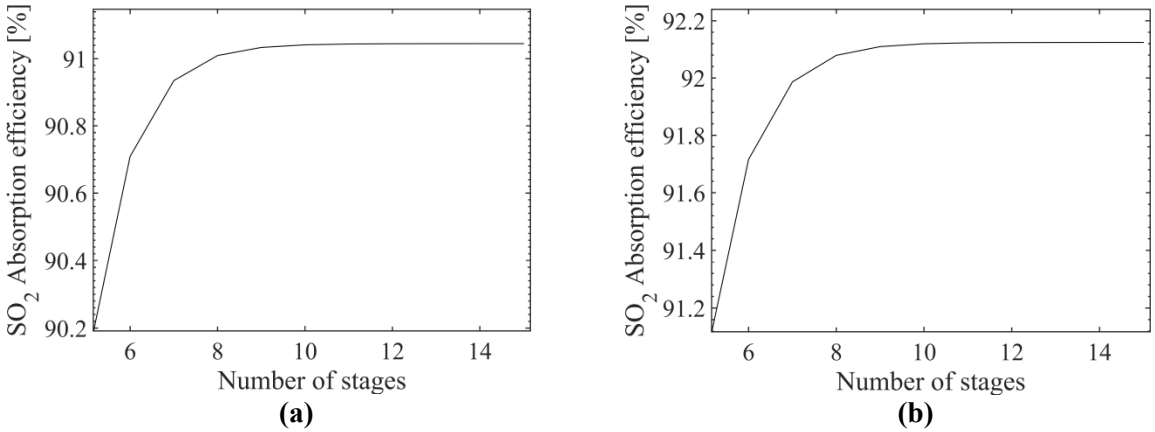

Figure 5.2: The SO_2 removal efficiency as a function of the total number of stages in the absorber column when the *standard model* (a) and *model 1* (b) is used.

5.1.2 Simulation of Absorption of SO_2

To investigate the absorption capacity and how the predictions of absorption in the *standard model* and *model 1* differ from each other, the lean buffer flow was varied. The absorber was simulated as illustrated in Figure 5.1.

The result from the simulation, where the lean buffer flow was varied, is shown in Figure 5.3.

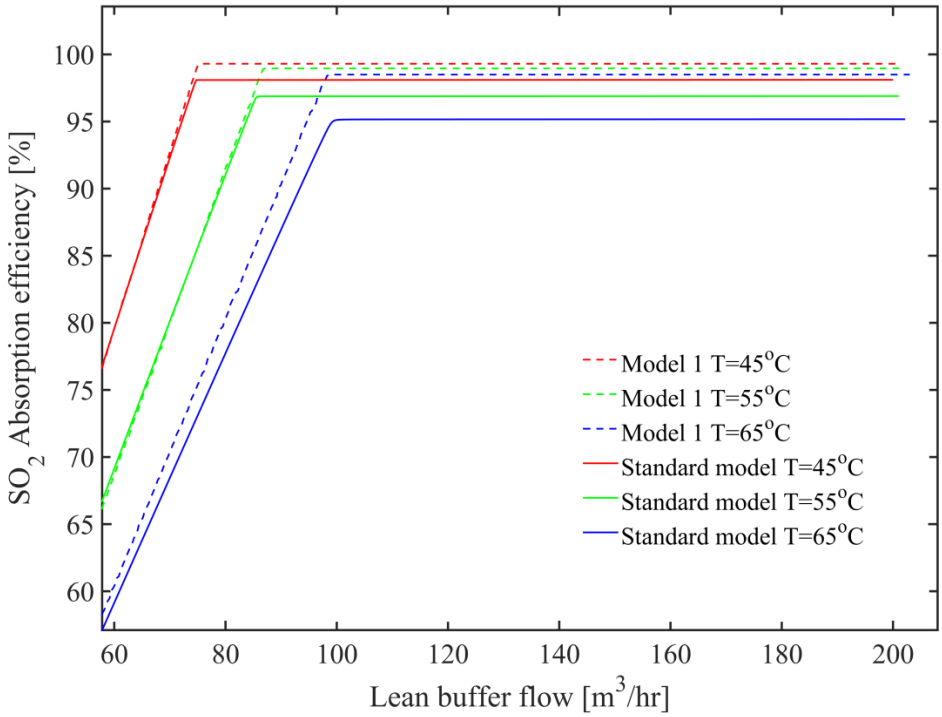

Figure 5.3: SO_2 absorption efficiency as a function of the lean buffer flow at 45 °C, 55 °C and 60°C.

Here, it can be seen that equilibrium is established after the breakpoint since there are no further improvement in SO_2 absorption efficiency when the lean buffer flow is further increased. For instance, at 55 °C the SO_2 absorption efficiency stabilises when the buffer flow is increased above 86.0 m^3/hr and 87.1 m^3/hr, in the *standard model* and *model 1*, respectively. At this flow the corresponding SO_2 absorption capacity is 96.9% and 99.0%, respectively. Thus, *model 1* shows the highest absorption capacity. The maximum absorption capacity is limited by the equilibrium behaviour shown in Figure 4.6.

It is also investigated whether the difference in absorption capacity has an impact on the maximum SO_2 concentration in the rich buffer stream. This is illustrated in Figure 5.4.

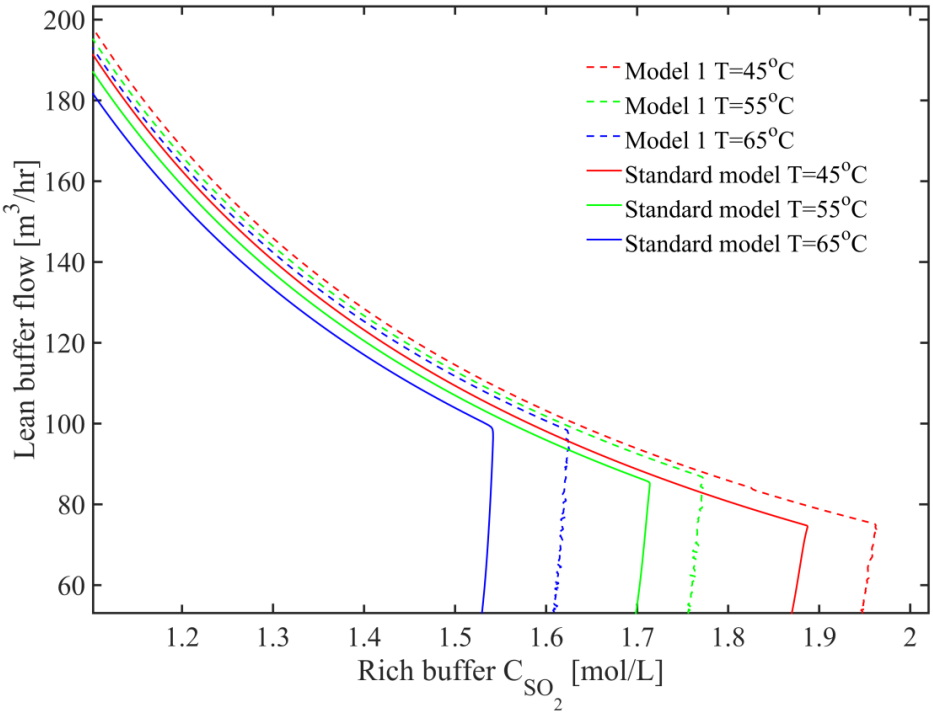

Figure 5.4: Lean buffer flow as a function of SO_2 concentration in rich buffer at 45 °C, 55 °C and 65°C.

Here, it can be seen that maximum SO_2 concentration at 55 °C is 1.71 mol_{SO2}/L in the *standard model* and 1.77 mol_{SO2}/L in *model 1*. These concentrations correspond to a lean buffer flow of 85 m^3/hr and 86 m^3/hr, respectively. Thus, higher rich loading is achieved in *model 1* and a higher buffer flow is used. However, the percentage difference in maximum SO_2 loading and the needed lean buffer flow is only 1.2% and 3.4%, respectively. Consequently, one can say that the difference in absorption capacity between the two models is very small. This small difference can also be seen from Figure 4.6 where the equilibrium partial pressures of SO_2 in the concentration range 1.3 mol_{SO2}/L to 1.8 mol_{SO2}/L in the *standard model* and *model 1* are quite similar. Furthermore from Figure 5.4, it can be seen that when lean buffer flow is increased above the flow needed to reach maximum SO_2 concentration, the SO_2 concentration in the rich buffer solution decreases.

Moreover, Figure 5.3 shows that the SO_2 absorption capacity increases with decreasing temperature. This increase in capacity is reasonable because SO_2 partial pressures at 30 °C are lower compared to partial pressures at 70 °C, as shown in Figure 4.6. To study how much absorption temperature affects the minimum lean buffer flow (and also pumping costs) required to reach 95% removal, the lean buffer flow were compared at 45 °C, 55 °C and 65

°C. Here, it was found that the minimum buffer flow will increase as the absorption temperature is increased. This is expected as maximum SO_2 concentration in the liquid decreases with temperature, as seen in Figure 5.4. For instance, at 95% SO_2 absorption efficiency in the *standard model*, the buffer flow needs to be increased by 16.1% and 38.0% at 55 °C and 65 °C, respectively, compared to the buffer flow needed at 45 °C. Thus, pumping cost will also increase with increased temperature. The same trend is also seen for *model 1*. The stream table where the absorption efficiency is 95% and the absorption temperature is 55 °C is shown in Appendix F.

5.1.3 Discussion

The operating conditions in Table 2.1, states that an SO_2 absorption efficiency of 95%, lean buffer flow of 115 m^3/hr and an absorption temperature of 55 °C results in an SO_2 concentration of 1.6 mol_{SO2}/L in the rich buffer stream. However, as seen from Figure 5.3 and in Appendix F, it was found that a lean buffer flow of 83.7 m^3/hr and 83.1 m^3/hr in the *standard model* and in *model 1*, respectively, is needed to achieve 95% absorption efficiency. At this efficiency the rich SO_2 concentration in the *standard model* and in *model 1* is 1.71 mol_{SO2}/L and 1.77 mol_{SO2}/L, respectively. Thus, assuming that the buffer solution used in the simulation gives comparable results with Table 2.1, they do not correspond. It seems that the simulation gives a too ideal picture of the absorption. In reality, larger buffer flow would be needed since it is not possible to reach equilibrium between gas and liquid phase. Thus, values in Table 2.1 may be realistic as absorption never is ideal. If kinetics for the sodium-phosphate-water-SO_2-system were included a more realistic simulation of absorption is probably possible to achieve.

5.2 Regeneration of SO_2

The regeneration unit in the Labsorb process consists of a heat exchanger, flash and a stripper as shown in Figure 1.1. The heater is located after the absorber and it is where SO_2 and water vapour is released from the SO_2-rich buffer solution. The evaporated SO_2 and water is then

separated from the buffer solution in the flash and SO_2 saturated with water exit the top of the stripper. In this study, the stripper is not included as its purpose is to separate water from SO_2. The ASPEN Plus simulation model is illustrated in Figure 5.5.

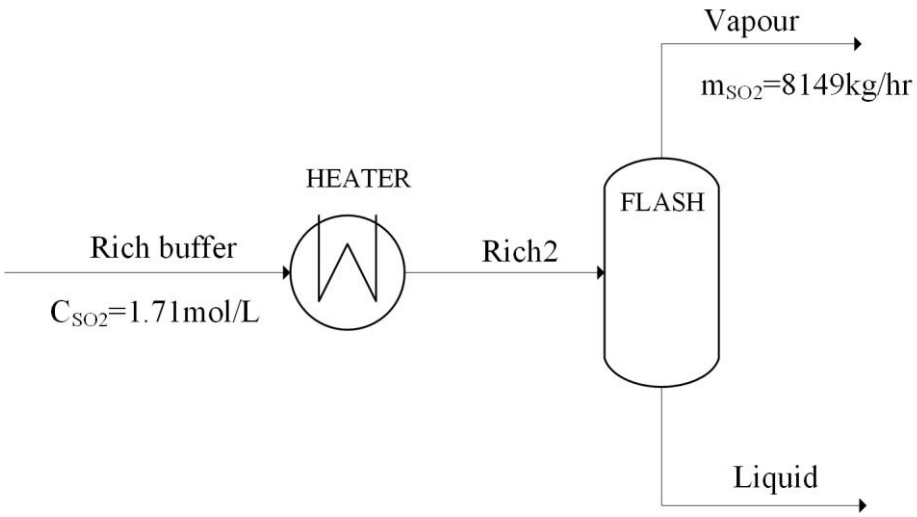

Figure 5.5: Illustration of the regeneration unit simulated in ASPEN Plus.

The goal of the study is to find energy efficient operating conditions for a plant with capacity of that presented in Table 2.1 where 95% removal efficiency is achieved, i.e. 8149 kg_{SO2}/hr is removed from the flue gas. The rich buffer stream, given in Appendix F, was used as input and the SO_2 loading of the rich buffer solution was always 1.71 mol_{SO2}/L. Although it was found from section 5.1 that 45 °C is the most suitable absorption temperature, 55 °C was used since it is given as an operating condition in Table 2.1. In case 45 ^{o}C would be used, the results would be approximately 600 kW higher heat load due to the energy needed to heat up the buffer solution from 45 °C to 55 ^{o}C.

To find energy efficient operating conditions for regeneration of SO_2 from the rich buffer flow, three different approaches were studied:

1. Stepwise removal of water
2. Pressure and temperature at the boiling point
3. Vary flow and temperature at atmospheric pressure

Below the three approaches are described. The *standard model* is described more in detail since the same behaviour can be seen in both models.

5.2.1 Stepwise Removal of Water

The feasibility of stepwise removal of water from the SO_2-rich buffer solution was studied by conducting flash calculations at 100 °C where 0%, 10% and 20% of the water was removed. The idea was based on the discussions related to how the solvent was regenerated during the first pilot campaigns at NTNU [37]. If the SO_2 partial pressure increased with decreasing water in the solution, it would be beneficial to remove water. However, as can be seen from Figure 5.6 below, the opposite trend applies to this system; partial pressure of SO_2 is decreasing as more water is removed from the solution. As a consequence, it looks as if there is not desirable to remove water from the SO_2-rich buffer solution to regenerate SO_2. The reason for this behaviour is not known, but could be because of possible non-realistic behaviour of the system in the *standard model* and in *model 1* in ASPEN Plus.

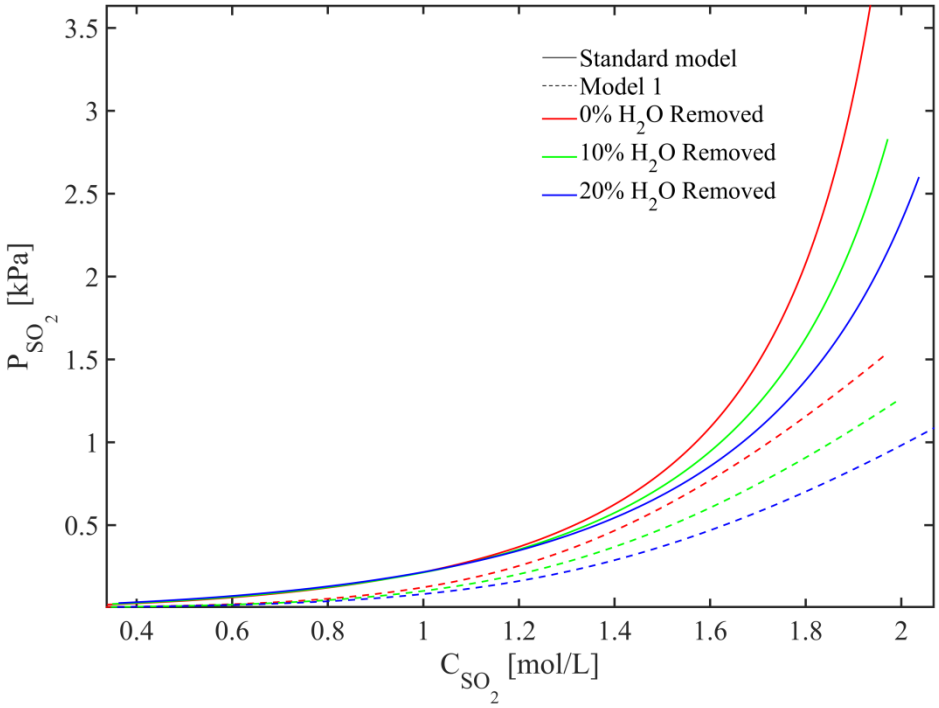

Figure 5.6: Partial pressure of SO_2 as a function of SO_2 concentration when 0%, 10% and 20% of the water is removed from the SO_2-rich buffer solution at 100°C.

Another explanation would be that solids are formed. This is further discussed in section 5.2.3. To test the possibility of formation of solids, the equilibrium curves, plotted in Figure 5.6, were generated again taking into account the possible formation of solids. The results showed that the SO_2 partial pressure increased as the amount of water is decreased. However, solids were formed in both models and there were great difficulties to get convergence.

5.2.2 Pressure and Temperature at the Boiling Point

The pressure and temperature were set so that the solution reached boiling point in the heater and in the flash. When total pressure and temperature were specified, in the *standard model*, it was discovered that huge amount of rich buffer flow was needed to achieve 95% SO_2 removal, as shown in Table 5.2.

Table 5.2: Temperature and pressure in heater/flash, required SO_2-rich buffer flow and energy in heater. 95% SO_2 removal efficiency is achieved.

T [°C]	P_{tot} [kPa]	Rich buffer flow [M m3/hr]	E_{heater} [MJ/kg$_{SO2}$]
110	119	2.93	66.7
120	165	4.25	117.1
130	225	5.55	178.5
140	301	6.91	257.1

The huge flow made the energy requirement unrealistically high. For instance, at 110 °C and 119 kPa, the energy requirement was found to be 66.7 MJ/kg$_{SO2}$. The reason for the very high energy requirement is explained by the VLE curve given in Figure 5.7 below. Here, the partial pressure of SO_2 is in the range 0.03-6.88 kPa at 110 °C, while the corresponding water vapour pressure and total pressure are 112-119 kPa and 119 kPa, respectively. Thus, the partial pressure of SO_2 is very low and a large amount of water has to be evaporated to regenerate SO_2.

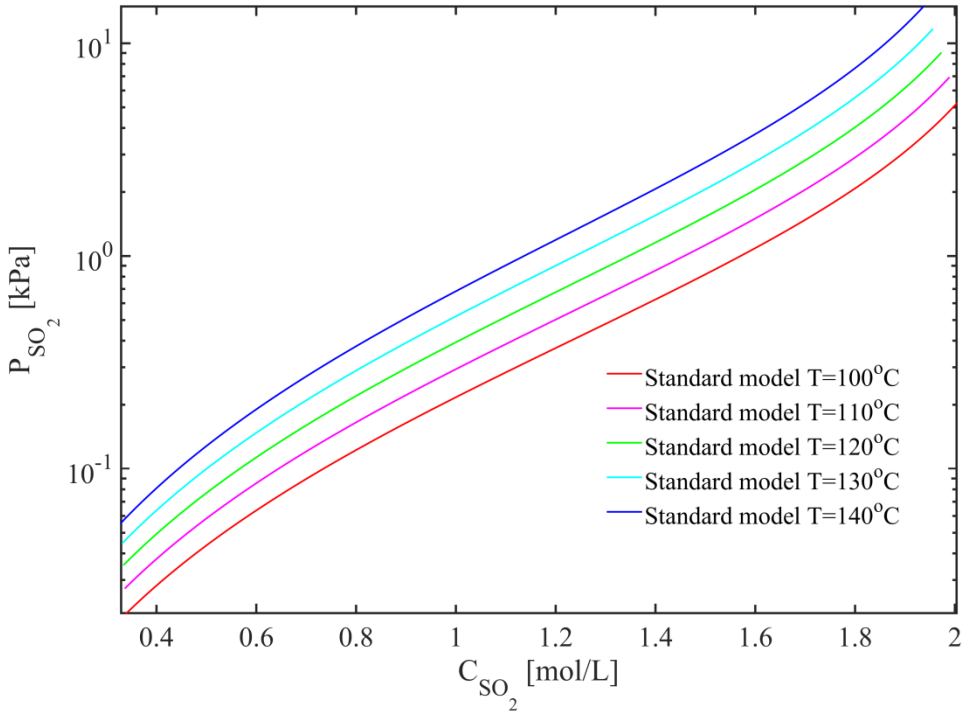

Figure 5.7: Partial pressure of SO2 as a function of SO_2 concentration in the aqueous phosphate water buffer solution 3/1/0.5.

The same behaviour is expected for model 1 but here the energy requirement is likely to be even higher. The reason is due to the lower SO_2 partial pressure as discussed in section 4.4.

Another reason for the high energy requirement would be that solids are formed and should be accounted for in ASPEN Plus. As mentioned above solids will be discussed in section 5.2.3. When solids were taken into account in the *standard model*, and the same approach was used, the energy requirement in the heater became considerably lower, around 1.8MJ/kg_{SO2}. However, significant amounts of solids were formed. In *model 1* there were difficulties to get convergence when solids were included.

5.2.3 Vary Flow and Temperature at Atmospheric Pressure

The SO_2-rich buffer flow and the temperature, in the heater and in the flash, were varied to achieve 95% SO_2 removal efficiency. The pressure was always atmospheric.

As a starting point the rich buffer flow given in Appendix F was used. Here, a temperature of 125.8 °C in the heat and in the flash was needed, in the *standard model*, in order to achieve 95% SO_2 removal. At this temperature 66% of the solution was converted to vapour, consisting of SO_2 and water, and the remaining solution remained in the liquid phase.

However, due to the low liquid fraction it was suspected that a solid phase should be present, but since formation of solids was not supposed to be relevant to the process, solid formation was not accounted for in the simulations. Potential solids which may form, as addressed in section 1.3, are Na_2HPO_4, NaH_2PO_4 and Na_2SO_4, and their hydrated forms.

To ensure that solids were not formed, the solubility data, given in section 2.5, were extrapolated and compared with the solubility calculated from the simulation results. The solubility was calculated using the equation below.

$$\text{solubility [g/100g } H_2O] = \frac{n_i \times M_i \times 100}{m_{H_2O}} \qquad 5.2$$

Here, n_i is mole flow of component i, M_i is molar weight of component i and m is mass flow of water. Values for mole flow of component i and mass flow of water was taken from the liquid-stream leaving the bottom of the flash, as seen from Figure 5.5.

By trial and error, the rich buffer flow that prevented solids to form, according to the calculated solubility and the literature, was found. The result when using the *standard model* is tabulated in Table 5.3.

Table 5.3: The rich buffer flow, temperature and energy requirement in the heater/flash and solubilities of Na_2HPO_4, NaH_2PO_4 and Na_2SO_4 using the *standard model*. 95% SO_2 removal efficiency is achieved.

Run	Rich buffer Flow [m^3/hr]	T [°C]	E_{heater} [MJ/kg_{SO2}]	Solubility Na_2HPO_4 [g/100g H_2O]	Solubility NaH_2PO_4 [g/100g H_2O]	Solubility Na_2SO_4 [g/100g H_2O]
1	98.7	125.8	19.8	239.8	121.3	47.9
2	109.1	122.8	20.9	184.4	108.7	39.2
3	127.3	119.7	22.7	133.7	96.3	31.0
4	138.2	118.5	23.6	115.4	91.4	28.0
5	145.5	117.8	24.3	106.4	88.8	26.5
6	214.8	114.1	29.7	63.2	74.3	18.9

Here, the red colour indicates that the solution is saturated, i.e. the calculated solubility is above the extrapolated solubility and solids are likely to precipitate. The green colour indicates that the solution is undersaturated, i.e. the calculated solubility is below the extrapolated solubility and solids may not precipitate. The transition from red to green colour occurs because from the simulations it can be seen that less water are evaporated from the

solution as the temperature decreases and the rich flow increases. Thus, the ratio calculated from equation 5.2 becomes smaller. In Table 5.3, run 4 is just below the extrapolated solubility to Na_2HPO_4 such that precipitation of solids in the solution may be prevented. When the rich buffer flow is further increased, the degree of undersaturation and also the energy requirement in the heater increases. For instance, at run 4 the energy requirement is 23.7 $MJ/kg_{SO2,}$ while at run 7 the energy requirement is 27.5 MJ/kg_{SO2}. Stream table for run 4 is presented in Appendix G.

The same trend is also seen for *model 1*. However, here the energy requirement is higher as the temperature needed to achieve 95% SO_2 removal is higher. For example, when the rich buffer flow is 98.7 m^3/hr, the temperature and energy required is 210 °C and 24.3 MJ/kg_{SO2}, respectively. However, it seems that there are non-realistic behaviour of the system in *model 1* as it is needed such high temperature to achieve 95% SO_2 removal at atmospheric pressure. In the literature it was stated that the atmospheric boiling point of the buffer solution was around 107 °C.

In addition, as discussed in section 4.4 it can be seen from the simulations that *model 1* is more temperature sensitive than the *standard model*. For instance, when the rich buffer flow is increased from 98 m^3/hr to138.2 m^3/hr, the temperature in *model 1* is decreased from 210 °C to 172°C, while the temperature in the *standard model* is decreased from 125.8 °C to118.5 °C. Thus, the temperature in *model 1* is decreased a factor of 1.22 while the temperature in the *standard model* is decreased a factor of 1.06.

Even though it seems that increasing the rich buffer flow prevents solids to form, one cannot be sure if it's true when solids are not accounted for in simulations due to the salting-out effect, addressed in section 1.3.3. Therefore, these solids were taken into account in the *standard model*: Na_2HPO_4, $Na_2HPO_4*2H_2O$, $Na_2HPO_4*7H_2O$, $Na_2HPO_4*12H_2O$, NaH_2PO_4, $NaH_2PO_4*H_2O$, $NaH_2PO_4*2H_2O$, Na_2SO_4 and $Na_2SO_3*10H_2O$. Regeneration of SO_2 was then simulated as shown in Figure 5.5 and the rich buffer flow equivalent to the flow in run 4, 5 and 6 from Table 5.3 was used as input. The result is summarized in table Table 5.4.

Table 5.4: The rich buffer flow, temperature and energy consumption in the heat exchanger/flash and amount of the solid $Na_2HPO_4*7H_2O$ formed using the *standard model*. 95% removal efficiency is achieved.

Run	Rich buffer Flow [m^3/hr]	T [°C]	E_{heater} [MJ/kg_{SO2}]	Solid $Na_2HPO4*7H_2O$. [kg/hr]
4	138.2	97.81	3.00	65803
5	145.5	97.70	3.02	67683
6	214.8	97.02	3.40	83828

As seen from the table above, huge amount of the solid $Na_2HPO_4*7H_2O$ are formed, and the amount is increasing as the rich buffer flow is increased. At run 4, the amount of solids containing phosphate is a factor of 6837 higher than what is observed at the Sannazzoro Refinery. The energy consumption is 3 MJ/kg_{SO2}, which is about a factor of 8 lower than in the simulation where solids are not accounted for. Stream table for run 4 is shown in Appendix G.

An extra level of complexity is added when solids are included into the simulation. Therefore, below are the solid-liquid solubility and the VLE of the sodium-phosphate-water-SO_2-system in the temperature range 30 °C to 105 °C investigated in the *standard model* in ASPEN Plus. Further, it is examined whether it is possible to achieve convergence in the absorber column when solids are accounted for in the simulation.

In Figure 5.8, is the solubility of the components in aqueous solution obtained from the *standard model* in ASPEN Plus compared to values from the literature [17, 18].

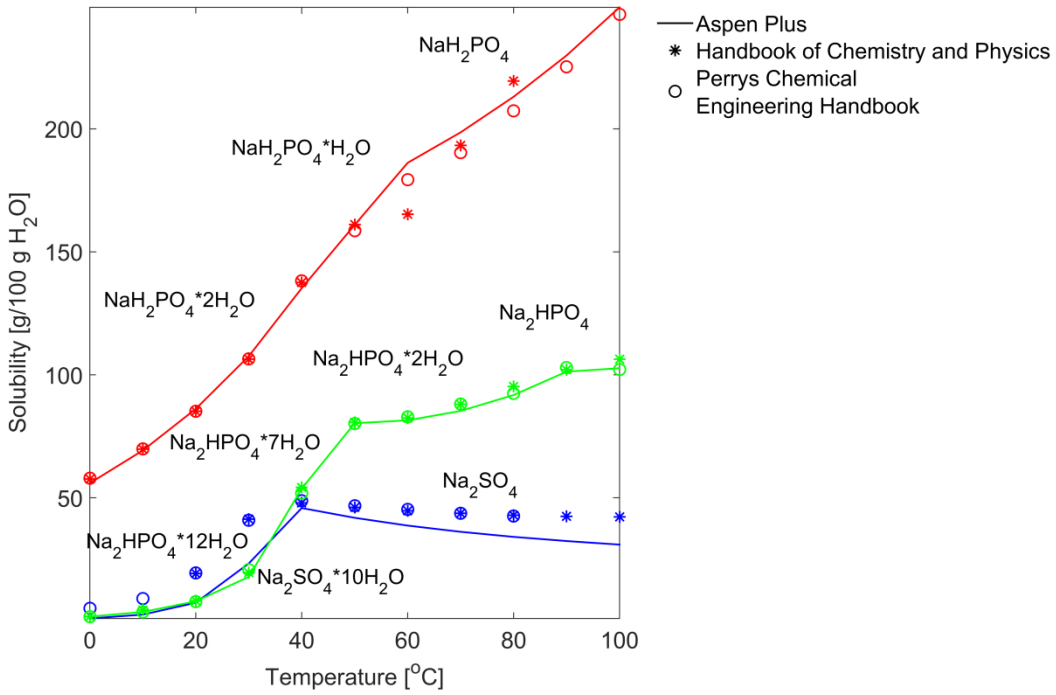

Figure 5.8: Solid-liquid solubility of Na_2HPO_4, NaH_2PO_4 and Na_2SO_4, and their hydrated form, in aqueous solution. The average deviation of the solubility's for Na_2HPO_4, NaH_2PO_4 and Na_2SO_4 is 3.4%, 2.5% and 31.4%, respectively

Here, it can be seen that the solubility is in good agreement with the literature data. The highest deviation is observed for Na_2SO_4.

In Figure 5.9, is the VLE in the temperature range 30 °C to 70 °C where solids are taken into account and not taken into account in the *standard model* compared with experimental data. Here, one can see that the VLE when solids are accounted for is nearly identical to the VLE when solid are not accounted for. However, a small deviation is observed at SO_2 concentrations below $0.7 mol_{SO2}/L$ at 30 °C where higher SO_2 partial pressures are reported. The fact that the two VLE curves are identical indicates that no solids are formed in the given temperature range.

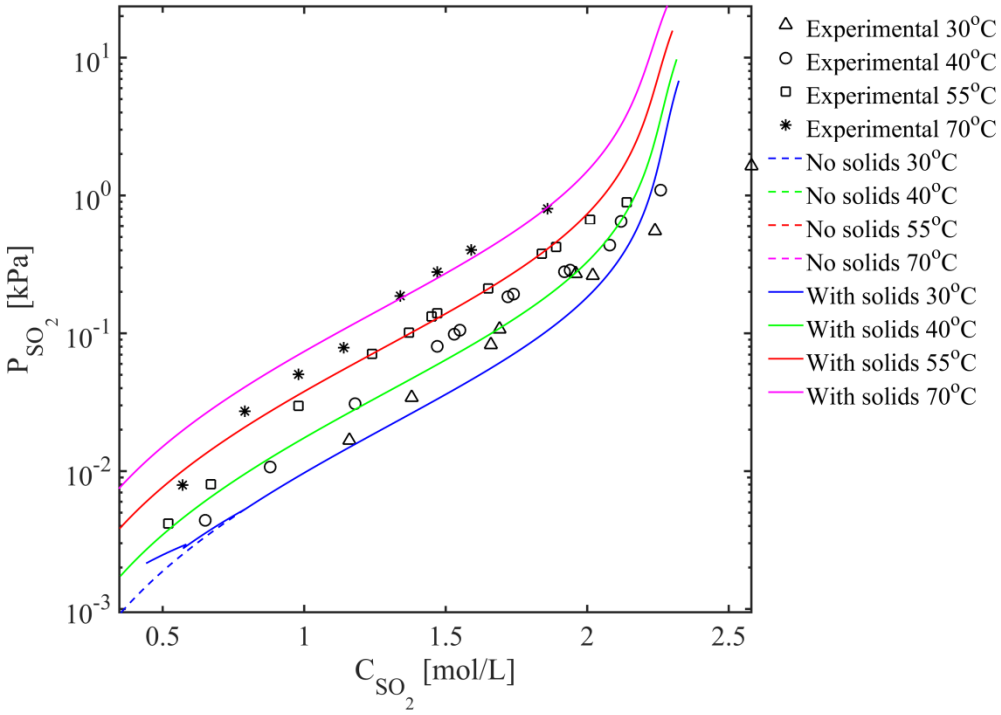

Figure 5.9: The partial pressure of SO_2 as a function of SO_2 concentration for buffer 3/1/0.5.

When the VLE were simulated in the temperature range 80 °C to 105 °C, as shown in Figure 5.10, it is observed that it is completely different from the VLE curve given in Figure 4.1. The change is due to the presence of solids. At all temperatures solids are present which causes the partial pressure of SO_2 to be very high.

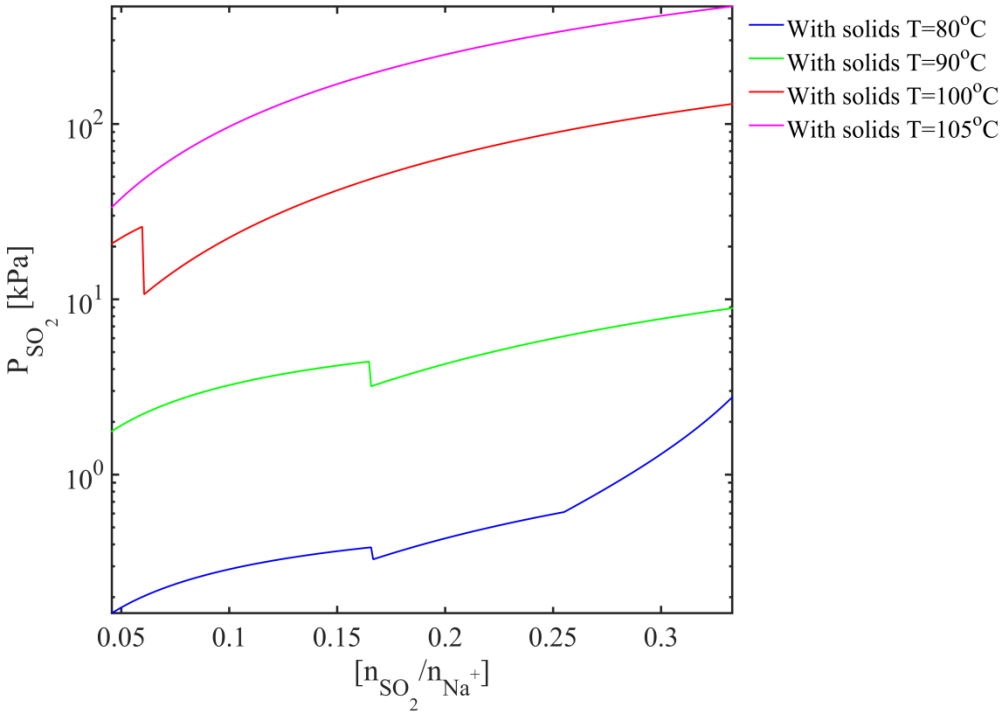

Figure 5.10: The partial pressure of SO_2 as a function of SO_2 concentration for buffer 3/1/0.5. Solids are accounted for in the *standard model*.

Further, from Figure 5.10 it is observed a pressure drop at 80 °C, 90 °C and 100 °C. The pressure drop is due to the transition from the solid $Na_2HPO_4*12H_2O$ to the solid $Na_2HPO_4*7H_2O$. Since $Na_2HPO_4*12H_2O$ contains more water compared to $Na_2HPO_4*7H_2O$, the amount of water in the solution will increase when the transition occurs. The increase of water in the solution causes the loading of SO_2 to decrease and thus also the partial pressure of SO_2. At 105 °C, a pressure drop is not present because it always contains the solid $Na_2HPO_4*7H_2O$.

To investigate whether it is possible to simulate absorption of SO_2 using the *standard model* when solids are accounted for, the absorber column was simulated as shown in Figure 5.1 and with operating conditions given in Table F.1. From the simulation, it appeared that the absorber failed to converge, and it was not found a reason to why [38]. However, a workaround, given in Appendix H, made it possible to simulate the absorber column with a warning. When the method given in Appendix H was applied it was confirmed that solids were not precipitating in the absorber column as suggested above.

5.2.4 Discussion

As there are no or limited experimental data to verify the simulated work, it is not possible to conclude which of the simulations that is closest to the reality. Thus, it is not possible to determine which operating conditions that are most energy efficient. Experimental VLE data at temperatures above 70 °C is missing such that simulated VLE at higher temperatures cannot be verified. Experimental water vapour pressure over the sodium-phosphate-water-SO_2 solution is not known and neither is density of the loaded and unloaded solution. In addition, solid-liquid solubility data for the system is not known. VLE, water vapour pressure, densities and solubility will greatly affect the simulated work and when they cannot be verified, it is not possible to know whether the regeneration is realistic.

When solids were taken into account, it was found that the solid-liquid solubility data in ASPEN Plus were in good agreement with the literature data, as shown in Figure 5.8. Thus, ASPEN Plus should be able to predict the behaviour of solids in the simulations. However, a recurring problem seemed to be that a significant amount of solids was formed and there were problems to achieve convergence. When regeneration of SO_2 was simulated in attempt 3, it was observed that a factor of 6837 more solids was formed in the simulation compared to the amount reported by the Sannazzoro Refinery. It was not expected that the differences would be so significant due to the good solubility agreement. However, it is not known whether solids are formed and dissolved within the process during operation. It is only reported how much solids are taken out. The solids which are formed may be dissolved when the condensed water from the stripper is mixed with the concentrated buffer solution. Moreover, if another buffer solution is used, less solids may be produced.

Further, from the literature review, it is given that the steam required to evaporate SO_2 from the buffer solution is 11 g/g_{SO2}. If one assumes that heat of evaporation is 2.24 MJ/kg_{steam}, the steam requirement corresponds to 24.6 MJ/kg_{SO2} when the SO_2 removal efficiency is 95%. From attempt 3, the energy requirement resulted from the simulation with solids and without solids, when the rich buffer flow was 138.2 m^3/hr, was 3.0 MJ/kg_{SO2} and 23.7 MJ/kg_{SO2}, respectively. Thus, the simulation where solids are not accounted for is closest to the literature value. However, this does not imply that the simulation without solids is trustworthy as there are no experimental data to verify this. The simulation where solids are accounted for has an energy requirement that is a factor of 8 lower compared to the value from the literature.

When regeneration of SO_2 was simulated, the rich SO_2 loading was always 1.71 mol_{SO2}/L, even if the rich buffer flow was increased. However, in section 5.1 it was found that the SO_2 concentration in rich buffer, at T=55 °C, decreased as the lean buffer flow increased above around 85m^3/hr. For instance, from Figure 5.3 it can be seen that when the lean buffer flow in the *standard model* is 138.2 m^3/hr, the rich SO_2 concentration is 1.4 mol_{SO2}/L, and not 1.7 mol_{SO2}/L as specified in the simulation. However, the intended purpose was to find ways to regenerate SO_2 and not to optimise with regard to SO_2 loading and buffer flow. If however one used 1.4 mol_{SO2}/L, the consequence would have been that the energy consumption would increase. The reason is because, as seen from Figure 4.7, the partial pressure of SO_2 is lower at low SO_2 concentrations compared to high SO_2 concentrations. Further, if one wants to optimise the buffer flow and SO_2 loading one need to simulate the absorber and regeneration unit in one part. In this work, they were simulated separately

Chapter 6

Conclusion

The scope of the thesis has been to develop an eNRTL thermodynamic model in ASPEN Plus that is able to describe experimental VLE data of the sodium-phosphate-water-SO_2-system. The result showed that this was achieved with an average deviation of 16.8%. The valid range of the eNRTL model is in the temperature range 40 °C to 70 °C and in the SO_2 concentration range 0.5 mol_{SO2}/L to 1.6 mol_{SO2}/L for buffer 3/1/0.5. Furthermore, the method used to improve VLE in ASPEN Plus works.

When absorption of SO_2 was studied, it was found that the absorption most likely was too ideal as it was not directly comparable to operating data from the literature. In spite of that, it was found that the absorption capacity increases with decreasing temperature and that the required flow of the lean buffer, entering the absorber column, increases with increasing absorption temperature. Further, it was found that no solids are formed in the absorber when solids are accounted for in the eNRTL model provided by ASPEN Plus.

Regeneration of SO_2 was studied as well and here it was not possible to conclude which operating conditions showed to be most energy efficient and closest to the reality. The reason is lack of experimental data in order to verify simulated work. At last, when simulating the Labsorb process, using ASPEN Plus, one should be aware of the possibility to form solids.

6.1 Recommendations for further work

While working with this thesis it became clear that more experimental work concerning the sodium-phosphate-water-SO_2-system is required. More experimental data will increase the understanding of the behaviour of the system, and be used to verify the simulated work.

Experimental VLE data above 70°C is required. Once high temperature VLE data are available one can improve the eNRTL model's representation of experimental data in ASPEN Plus and obtain a wider validity range.

Further, experimental solid-liquid solubility data of the system at low and high temperatures is required. Experimental solubility data will reveal the possibility for solid formation. Experimental density data and kinetic study are also important. By having kinetic data of the system one can use the rate-based RadFrac column in ASPEN Plus, instead of the equilibrium-based RadFrac column. The rate-based approach accounts for the interphase mass and heat transfer processes and will represent a more realistic simulation.

Bibliography

1. Srivastava, R.K.a.J.W., *Flue Gas Desulfurization: The State of the Art.* Journal of The Air & Waste Management Association, 2001. 51: p. 1676-1688.
2. Nordstrand, D., Duong Dao, N. B., and Miller B. G., *Chapter 9 - Post Combustion Emissions Control*, in *Combustion Engineering Issues for Solid Fuel Systems*, B.G.M.A. Tillman, Editor. 2008, Academic Press: Burlington. p. 341-391.
3. The International Energy Agency, *Key World Energy Statistic.* 2014.
4. Bernhardsen, I., *Removal of SO2 from flue gas.* Specialisation project NTNU, 2014.
5. Amoroso, A., *RefinARS Technological and methodological approach*, ENI Sannazzaro Refinery, Editor., ENI Refining and Marketing Division: Italy.
6. Erga, O.a.F., A.,, *The Elsorb process: A new regenerable prcocess for SO2 recovery.* Icheme symposium 1993. 131: p. 197-209.
7. Eagleson, S., Confuorto, N. and Pedersen, B.,, *Labsorb: a regenerable wet scrubbing process for controlling SO2 emissions*, in *Digital Refining*. 2001.
8. Erga, O., *A new regenerable process for the recovery of SO2.* Chemical Engineering Technology, 1988. 11: p. 402-407.
9. Erga, O., and Confuorto, N., *SO2 from combustion gases -the Labsorbt process*, in *Sulphur 2002*. October 2002: Vienna, Austria.
10. Weisenberger, S., and Schumpe, A.,, *Estimation of Gas Solubilities in Salt Solutions at Temperatures from 273 K to 363 K.* AIChE, 1996. 42(1): p. 298-300.
11. Amoroso A. and Confuorto N., *Report on the Labsorb regenerative SO2 scrubbing system application at the Eni SpA refinery FCCU in Sannazzaro, Italy*, in *Digital Refining* 2004.
12. Weaver, E., *Evaluating wet scrubbers*, in *Digital Refining*. 2006.
13. Olav Erga, *SO2 utvinning i Norilsk.* Erga Consulting, year unknown,.
14. Hove, H.E., *Master thesis: Gas liquid model for SO2: study of the regenerable Elsorb process*. 2013, NTNU.
15. Personal communivation with Prof. Olav Erga.
16. Haynes, W.M., *CRC Handbook of Chemistry and Physics, 95th Edition.* 2014: p. 5-144.
17. Haynes, W.M., *CRC Handbook of Chemistry and Physics, 95th Edition.* 2014: p. 5-194.
18. Perry, R.H., D.W. Green, and J.O. Maloney, *Perry's Chemical Engineers' Handbook.* 1999: p. 2-123.
19. Smith, J.M.a.V.N., H.C., *Introduction to chemical engineering thermodynamics.* 1987. 4th Edition: p. 297-326.
20. Geankoplis, C.J., *Transport Processes and Separation Process Principles: Includes Unit Operations.* 2003: p. 628-696.
21. Warberg T.H., *Den termodynamiske arbeidsboken.* 2006: p. 136-169.
22. Gilbert Newton, L., *The Law of Physico-Chemical Change.* Proceedings of the American Academy of Arts and Sciences, 1901. 37(3): p. 49-69.
23. Renon, H. and J.M. Prausnitz, *Local compositions in thermodynamic excess functions for liquid mixtures.* AIChE Journal, 1968. 14(1): p. 135-144.
24. Gmehling, J., J. Li, and M. Schiller, *A modified UNIFAC model. 2. Present parameter matrix and results for different thermodynamic properties.* Industrial & Engineering Chemistry Research, 1993. 32(1): p. 178-193.
25. Abrams, D.S. and J.M. Prausnitz, *Statistical thermodynamics of liquid mixtures: A new expression for the excess Gibbs energy of partly or completely miscible systems.* AIChE Journal, 1975. 21(1): p. 116-128.

26. Fischer, K. and J. Gmehling, *Further development, status and results of the PSRK method for the prediction of vapor-liquid equilibria and gas solubilities.* Fluid Phase Equilibria, 1996. 121(1–2): p. 185-206.
27. Wilson, G.M., *Vapor-Liquid Equilibrium. XI. A New Expression for the Excess Free Energy of Mixing.* Journal of the American Chemical Society, 1964. 86(2): p. 127-130.
28. Gmehling, J., D. Tiegs, and U. Knipp, *A comparison of the predictive capability of different group contribution methods.* Fluid Phase Equilibria, 1990. 54(0): p. 147-165.
29. Chen, C.-C., et al., *Local composition model for excess Gibbs energy of electrolyte systems. Part I: Single solvent, single completely dissociated electrolyte systems.* AIChE Journal, 1982. 28(4): p. 588-596.
30. Chen, C.-C. and Y. Song, *Generalized electrolyte-NRTL model for mixed-solvent electrolyte systems.* AIChE Journal, 2004. 50(8): p. 1928-1941.
31. Aspen Technology, I., *Aspen physical property system.* 2014.
32. Chen, C.-C., Y. Zhu, and L.B. Evans, *Phase Partitioning of Biomolecules: Solubilities of Amino Acids.* Biotechnology Progress, 1989. 5(3): p. 111-118.
33. Hertzberg, T.a.M., T, *MODFIT for MatLab: Parameter Estimation in a General Nonlinear Multireponse Model*. 1998, Norwegian University of Science and Technology: Trondheim, Norway.
34. Chen, C.C., *A local composition model or the excess gibbs energy of aqueous electrolyte systems.* AIChE, 1986. 32(3): p. 444-454.
35. Personal communication with Hanna Knuutila.
36. Wang, J.-F., Li, Chun-Xi, Zi-Hao, Zi-Jia and Jiang, Yan-Bin, *Vapor pressure measurement for water, methanol, ethanol, and their binary mixtures in the presence of an ionic liquid 1-ethyl-3-methylimidazolium dimethylphosphate.* Fluid Phase Equilibria, 2007. 255(2): p. 186-192.
37. Personal communications with Olav Juliussen and Hallvard Svendsen.
38. Consultation with Aspentech support center.

Appendix A Hand Calculations

In Appendix A, hand calculations is performed to calculate the amount of SO_2 absorbed using operating conditions given in Table 2.1

Hand calculations based on the SO_2 concentration in lean and rich buffer:

Absorbed SO_2:	$(1.6-0.5)\frac{kmol}{m^3}\times 115 m^3 = 126.5 kmol$	6.1

Hand calculations based on the difference between the fraction of SO_2 in the flue gas and in the clean gas:

Difference in inlet and outlet SO_2 concentration:	$\left(\frac{0.0003}{1}-\frac{0.00017}{1}\right)\times 10^6 \frac{Nm^3}{hr} = 2830\frac{Nm^3}{hr}$	6.2
Absorbed SO_2:	$\frac{2830 Nm^3/hr}{22.414 Nm^3/kmol} = 126.3 kmol/hr$	6.3

Hand calculations based on the fraction of SO_2 in the flue gas and the SO_2 removal efficiency:

Flue gas converted from Nm^3 to kmol:	$\frac{10^6 Nm^3/hr}{22.414 Nm^3/kmol} = 44614.97 kmol/hr$	6.4
Mole flow SO_2:	$44614.97 kmol/hr \times 0.003 = 133.844 kmol$	6.5
Absorbed SO_2:	$133.844 kmol \times 95\% = 127.156 kmol$	6.6

Hand calculations show that the amount SO_2 absorbed is 126.5 kmol/hr, 126.3 kmol/hr and 127.125 kmol/hr, depending on how it is calculated. The calculated values deviates 0.4% from the tabulated value, 127 kmol/hr.

Appendix B VLE Simulated in the Standard Model

In Appendix B, VLE curves for buffer 2.5/1.25/0.5, 2.5/0.83/0.5 and 2.5/0.25/0.5, simulated in the *standard model* in ASPEN Plus, are presented. In Figure B.1, B.2 and B.3, the experimental VLE data in the temperature range 40 °C to 70 °C is compared with the *standard model* for buffer 2.5/1.25/0.5, 2.5/0.83/0.5 and 2.5/0.25/0.5, respectively. When the notation buffer 3/1/0.5 is used, it denotes that the buffer composition is $C_{Na_2HPO_4}$ = 3 mol/L, $C_{NaH_2PO_4}$ = 1 mol/L and $C_{Na_2SO_4}$ = 0.5 mol/L.

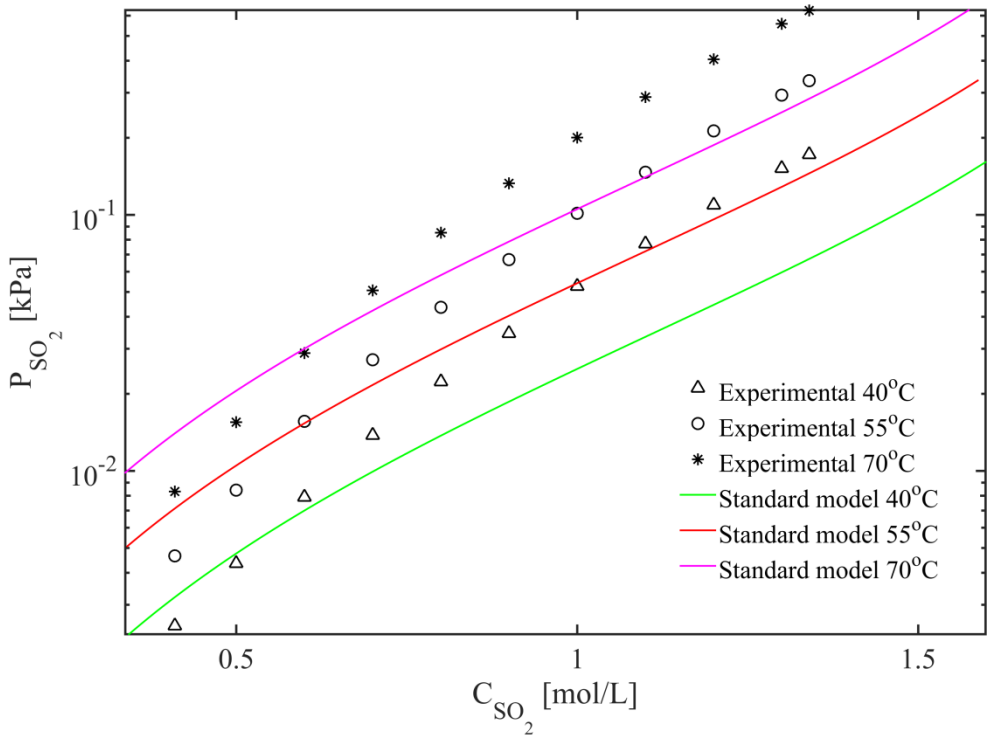

Figure B.1: The partial pressure of SO_2 as a function of the SO_2 concentration in the aqueous phosphate buffer solution 2.5/1.25/0.5. The average deviation of the *standard model* is 40.4%.

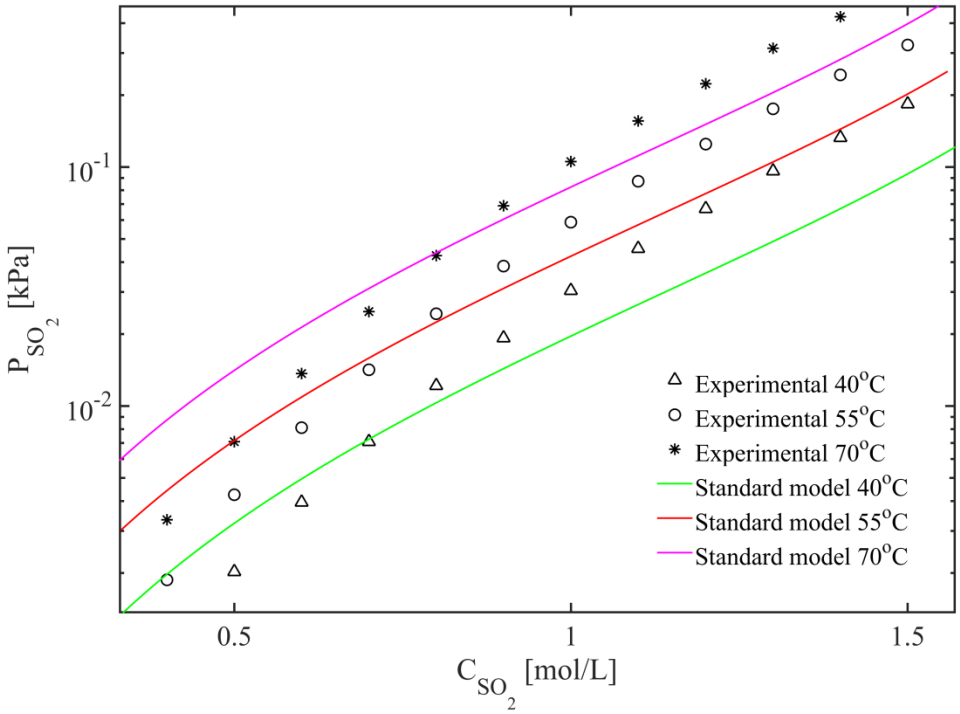

Figure B.2: The partial pressure of SO_2 as a function of the SO_2 concentration in the aqueous phosphate buffer solution 2.5/0.83/0.5. The average deviation of the *standard model* is 41.7%

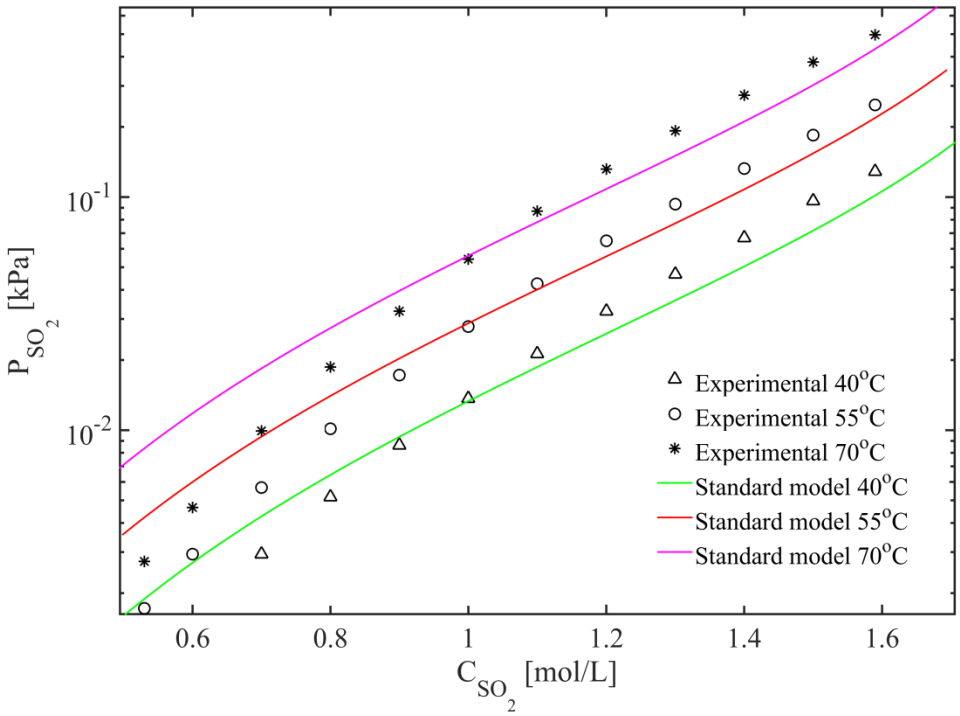

Figure B.3: The partial pressure of SO_2 as a function of the SO_2 concentration in the aqueous phosphate buffer solution 2.5/0.25/0.5. The average deviation of the *standard model* is 37.3%

Appendix C Artificial VLE Data

In Appendix C, the parameters used in the soft model function, given in equation 4.3, and artificial VLE data compared with experimental data are presented for buffer 2.5/1.25/0.5, 2.5/0.83/0.5, 2.5/0.25/0.5 and 3/1/0.5.

C.1 Artificial VLE Data for Buffer 2.5/1.25/0.5

The parameters used in the soft-model function for buffer 2.5/1.25/0.5 are presented in Table C.1, and artificial VLE data in the temperature range 40 °C to 105 °C compared with experimental data is presented in Figure C.1.

Table C.1: Parameters for buffer 2.5/1.25/0.5 used in the soft model function

Parameter	Value
A	3.77
B	0.35
k_1	-5276.49*(1/T) + 21.61
k_2	exp(13764.80*(1/T) - 50.35)
k_3	-12496.01*(1/T) + 43.16

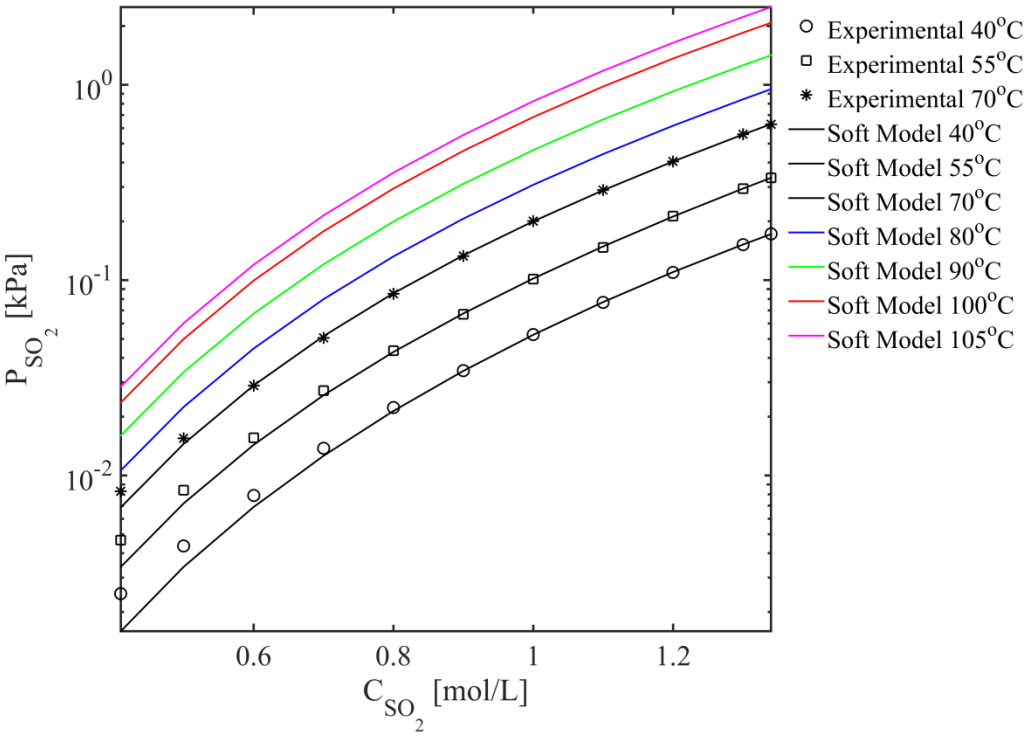

Figure C.1: The partial pressure of SO_2 as a function of the SO_2 concentration in the aqueous phosphate buffer solution 2.5/1.25/0.5. The average deviation of the soft model is 5.2%

C.2 Artificial VLE Data for Buffer 2.5/0.83/0.5

The parameters used in the soft-model function for buffer 2.5/0.83/0.5 are presented in Table C.2, and artificial VLE data in the temperature range 40 °C to 105 °C compared with experimental VLE data is presented in Figure C.2.

Table C.2: Parameters for buffer 2.5/0.83/0.5 used in the soft model function

Parameter	Value
A	5.83
B	-34.76
k_1	-7359.37*(1/T) + 60.49
k_2	exp(1259.51*(1/T) - 6.11245275)
k_3	-320.29*(1/T) + 1.31

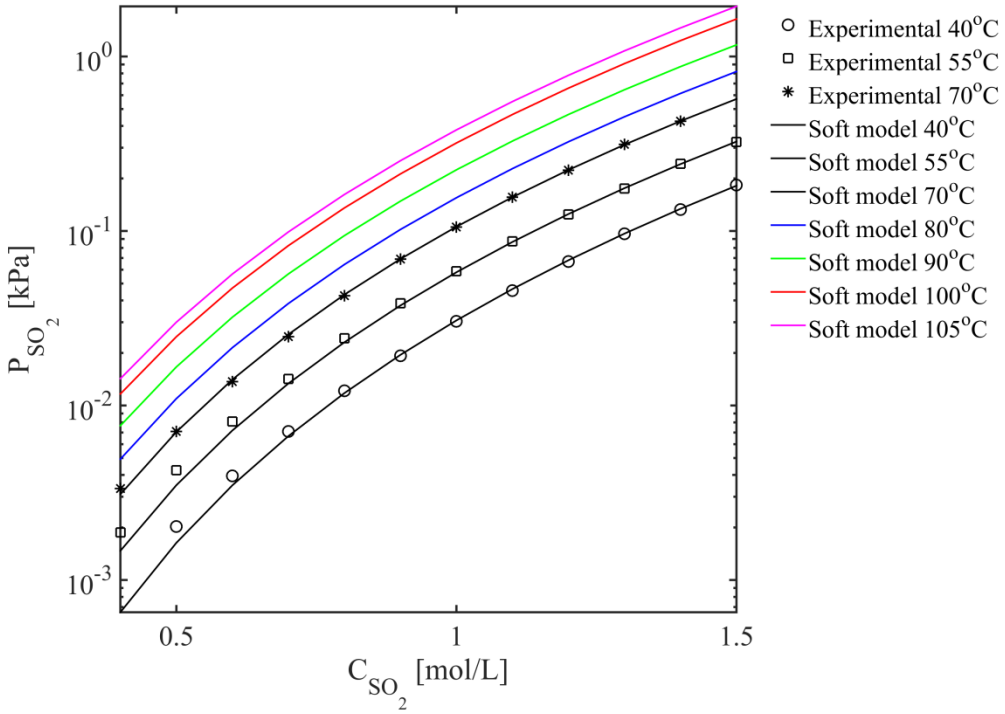

Figure C.2: The partial pressure of SO_2 as a function of the SO_2 concentration in the aqueous phosphate buffer solution 2.5/0.83/0.5. The average deviation of the soft model is 4.0%.

C.3 Artificial VLE Data for Buffer 2.5/0.25/0.5

The parameters used in the soft-model function for buffer 2.5/0.25/0.5 are presented in Table C.3 and artificial VLE data in the temperature range 40 °C to 105 °C compared with experimental data is presented in Figure C.3.

Table C.3: Parameters for buffer 2.5/0.25/0.5 used in the soft model function

Parameter	Value
A	4.72
B	-0.22
k_1	-5384.66*(1/T) + 22.84
k_2	exp(-332706.20*(1/T) + 1070.73)
k_3	218626.60*(1/T) - 702.86

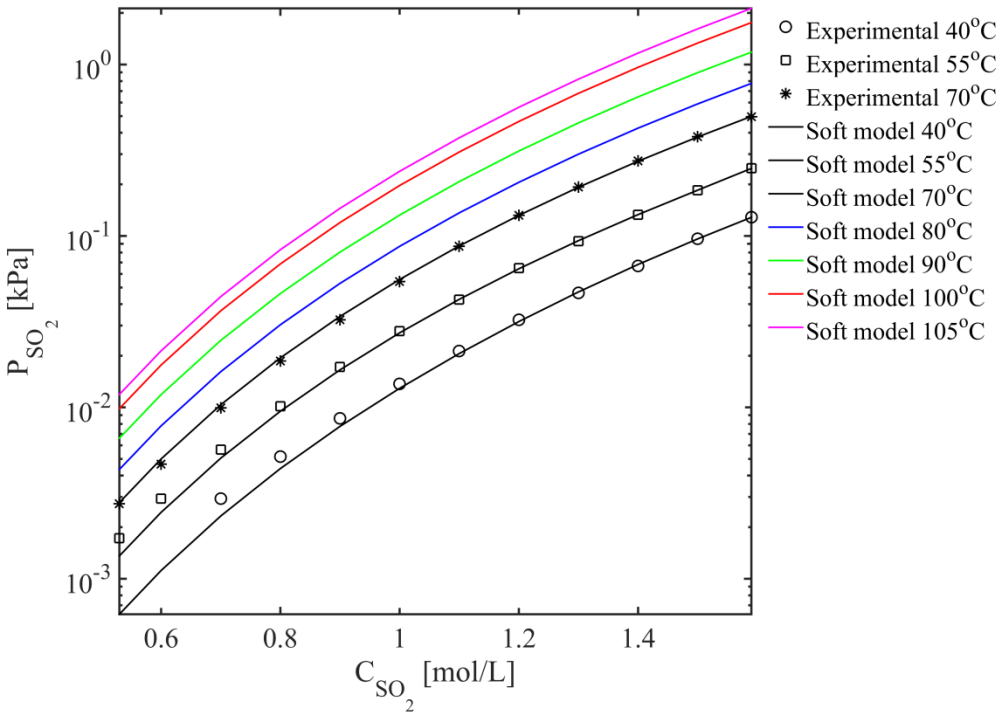

Figure C.3: The partial pressure of SO_2 as a function of the SO_2 concentration in the aqueous phosphate buffer solution 2.5/0.25/0.5. The average deviation of soft model is 4.5%.

Appendix D Binary Parameters

In Appendix D, the binary parameters A, B, C and D used in the eNRTL model in ASPEN Plus are presented. The fitted binary parameters, A and B in *model 1* and *2* and its value in the *standard model* are presented in Table D.1. The fitted binary parameters, C and D, in *model 1* and *2* and its value in the *standard model* are presented in Table D.2 and Table D.3, respectively.

Table D.1: The binary parameters A and B for the H_2O-SO_2-binary system, $\alpha = 0.2$

Parameter	Component i	Component j	Standard model	Model 1	Model 2
A_{ij}	H_2O	SO_2	1	4.6298	-3.3942
A_{ij}	SO_2	H_2O	1	3.081	-3.2129
B_{ij}	H_2O	SO_2	1	596.8758	3360.295
B_{ij}	SO_2	H_2O	1	970.2561	2064.494

Table D.2: The binary parameter C for the sodium-phosphate-water-SO_2-system, $\alpha = 0.2$

Parameter	Component i	Component j	Standard model	Model 1	Model 2
C_{ij}	H_2O	$(Na^+ H_2PO_4^-)$	8.275736	2.323	-8.4872
C_{ij}	$(Na^+, H_2PO_4^-)$	H_2O	-3.89122	-1.3644	0.12833
C_{ij}	H_2O	$(Na+ HPO_4^{2-})$	7.475	-5.5929	-4.1692
C_{ij}	(Na^+, HPO_4^{2-})	H_2O	-3.581	3.7718	2.6437
C_{ij}	H_2O	(Na^+, HSO_3^-)	8.799737	2.1907	-11.8158
C_{ij}	$(NA+ HSO_3^-)$	H_2O	-4.4715	0.91531	9.2395
C_{ij}	H_2O	(Na^+, SO_3^{2-})	12.12477	-2.2646	7.1012
$C\tau_{ij}$	(Na^+, SO_3^{2-})	H_2O	-5.73349	-1.3665	8.5986
C_{ij}	H_2O	(Na^+, SO_4^{2-})	1.9545	-1.0652	4.1908
C_{ij}	(Na^+, SO_4^{2-})	H_2O	-2.03326	-1.9342	9.688

Table D.3: The binary parameter D for the sodium-phosphate-water-SO_2-system, α=0.2

Parameter	Component i	Component j	Standard model	Model 1	Model 2
D_{ij}	H_2O	(Na^+ $H_2PO_4^-$)	0	864.9824	90.5702
D_{ij}	(Na^+, $H_2PO_4^-$)	H_2O	0	-663.852	-847.399
D_{ij}	H_2O	(Na+ HPO_4^{2-})	0	2144.064	1443.014
D_{ij}	(Na^+, HPO_4^{2-})	H_2O	0	1341.555	140.3334
D_{ij}	H_2O	(Na^+, HSO_3^-)	0	1371.616	-1685.3
D_{ij}	(NA+ HSO_3^-)	H_2O	0	-1012.2	-1828.9
D_{ij}	H_2O	(Na^+, SO_3^{2-})	0	-24.9918	-398.207
D_{ij}	(Na^+, SO_3^{2-})	H_2O	0	1501.165	-437.302
D_{ij}	H_2O	(Na^+, SO_4^{2-})	1762.185	-561.762	3853.303
D_{ij}	(Na^+, SO_4^{2-})	H_2O	-537.968	-623.618	-2666.12

Appendix E VLE Simulated in Model 1 and 2

In Appendix E, VLE curves are simulated in two modified eNRTL models; *model 1* and *model 2*. *Model 1* has fitted binary parameters from experimental data and *model 2* has fitted binary parameters from experimental data and artificial VLE data in the temperature range 80 °C to 105 °C. In section E.1 is *model 1* and *2* compared in the temperature range 40 °C to 70 °C and in section E.2 is *model 2* compared with artificial VLE data in the temperature range 80 °C to 105 °C.

E.1 VLE Compared in the Temperature Range 40 °C to 70 °C

In Figure E.1, E.2 and E.3, the experimental data in the temperature range 40 °C to 70 °C is compared with VLE data obtained from *model 1* and *2* for buffer 2.5/1.25/0.5, 2.5/0.83/0.5 and 2.5/0.25/0.5, respectively

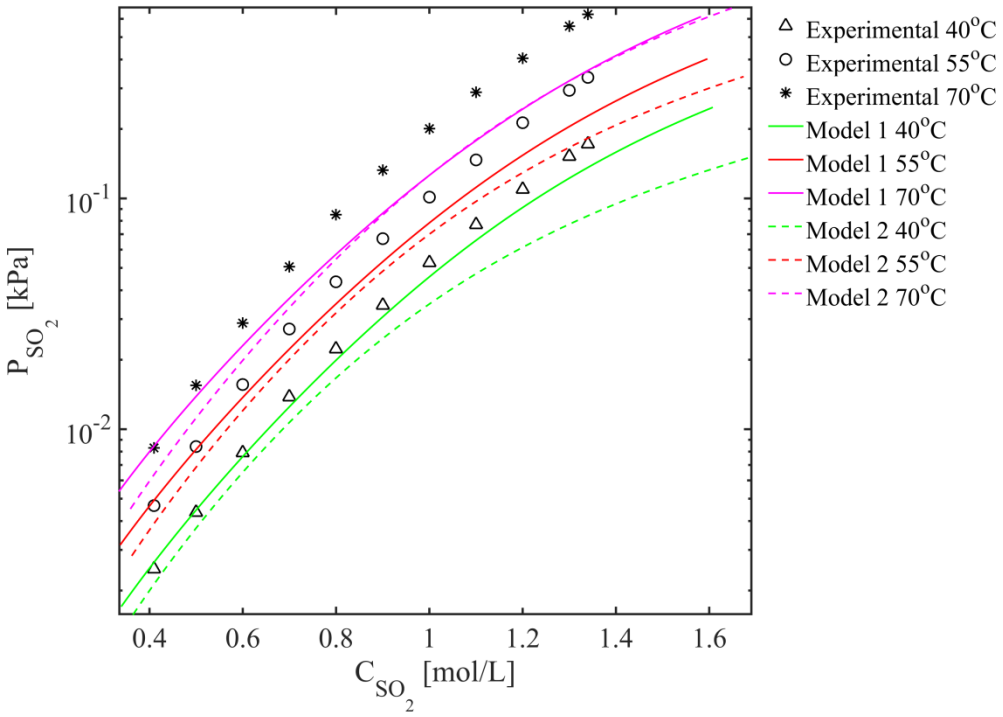

Figure E.1: The partial pressure of SO_2 as a function of the SO_2 concentration in the aqueous phosphate buffer solution 2.5/1.25/0.5. The average deviation of the *model 1* and *2* is 19.5% and 31.6%, respectively.

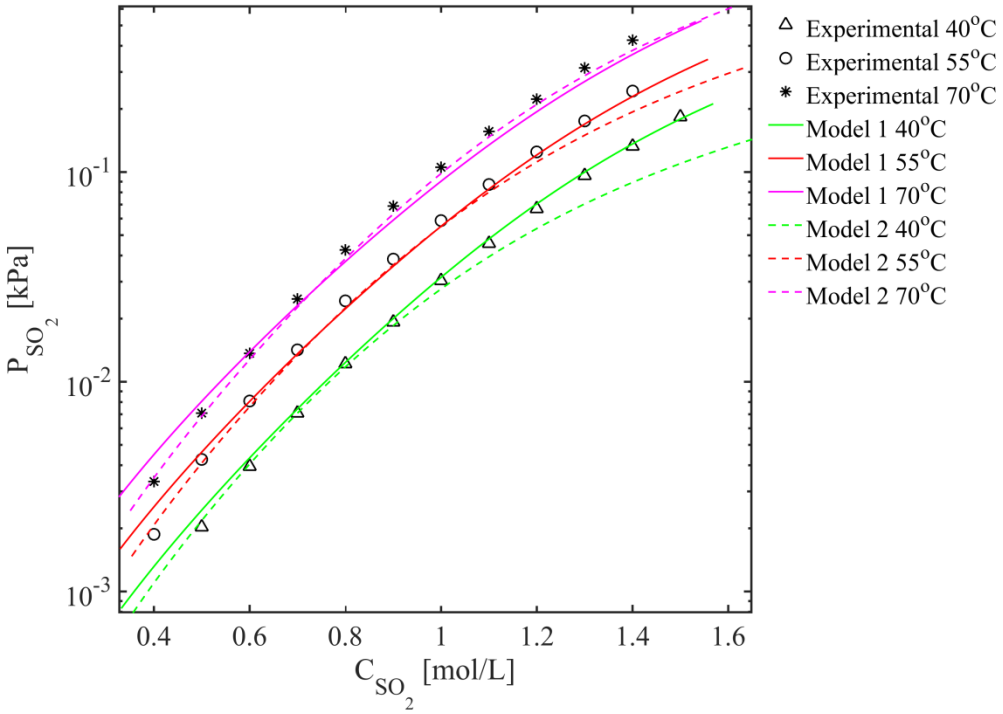

Figure E.2: The partial pressure of SO_2 as a function of the SO_2 concentration in the aqueous phosphate buffer solution 2.5/0.83/0.5. The average deviation of *model 1* and *2* is 9.2% and 10.0%, respectively.

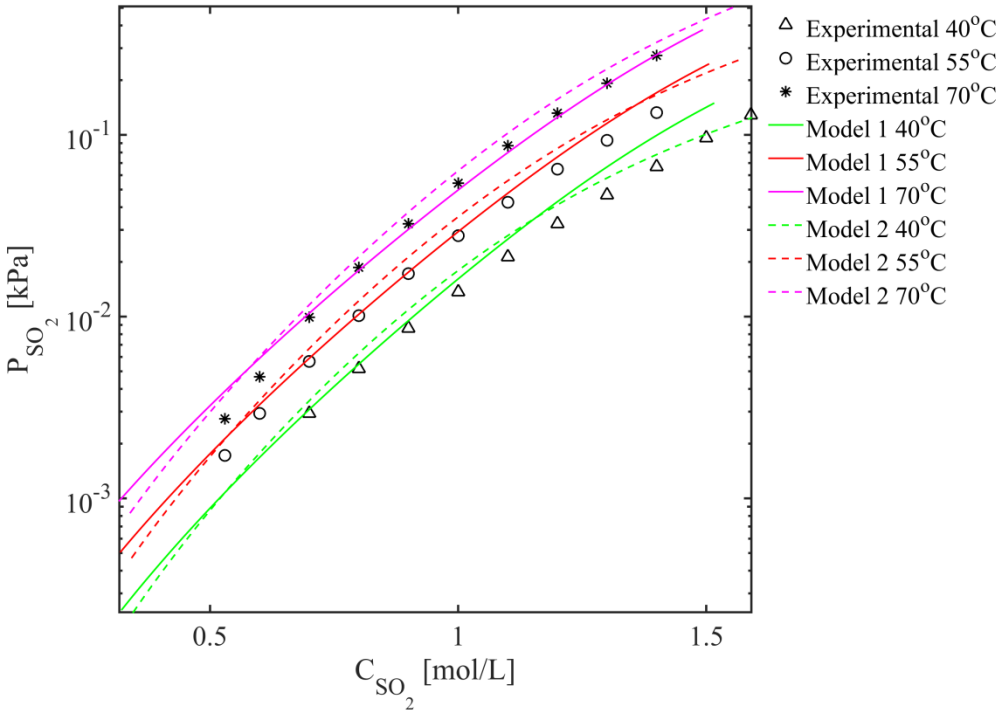

Figure E.3: The partial pressure of SO_2 as a function of the SO_2 concentration in the aqueous phosphate buffer solution 2.25/0.25/0.5. The average deviation of *model 1* and *2* is 18.5% and 21.4%, respectively.

E.2 VLE simulated in *Model 2* in the Temperature Range 80 °C to 105 °C

In Figure E.4, E.5 and E.6, the artificial VLE data in the temperature range 80 °C to 105 °C is compared with VLE data obtained from *model 2* for buffer 2.5/1.25/0.5, 2.5/0.83/0.5 and 2.5/0.25/0.5, respectively.

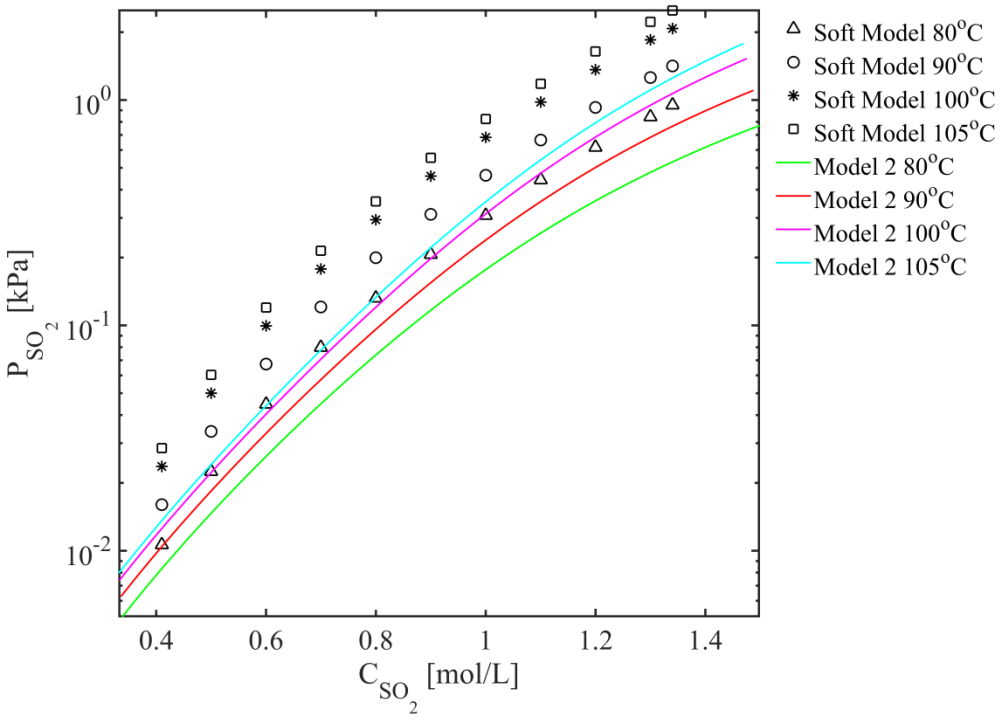

Figure E.4: The partial pressure of SO_2 as a function of the concentration of SO_2 in the aqueous phosphate buffer solution 2.5/1.25/0.5. The average deviation of *model 2* is 49.2%.

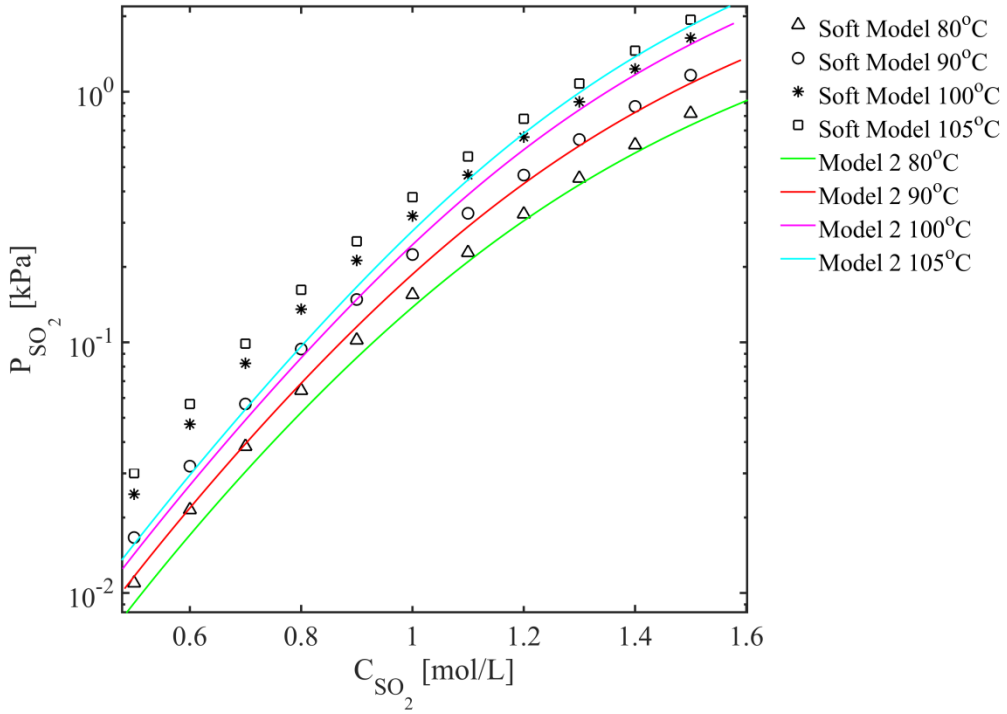

Figure E.5: The partial pressure of SO_2 , P_{SO2}, as a function of the concentration of SO_2 ,C_{SO2}, in the aqueous phosphate buffer solution 2.5/0.83/0.5. The average deviation of -*model 2* is 19.3%.

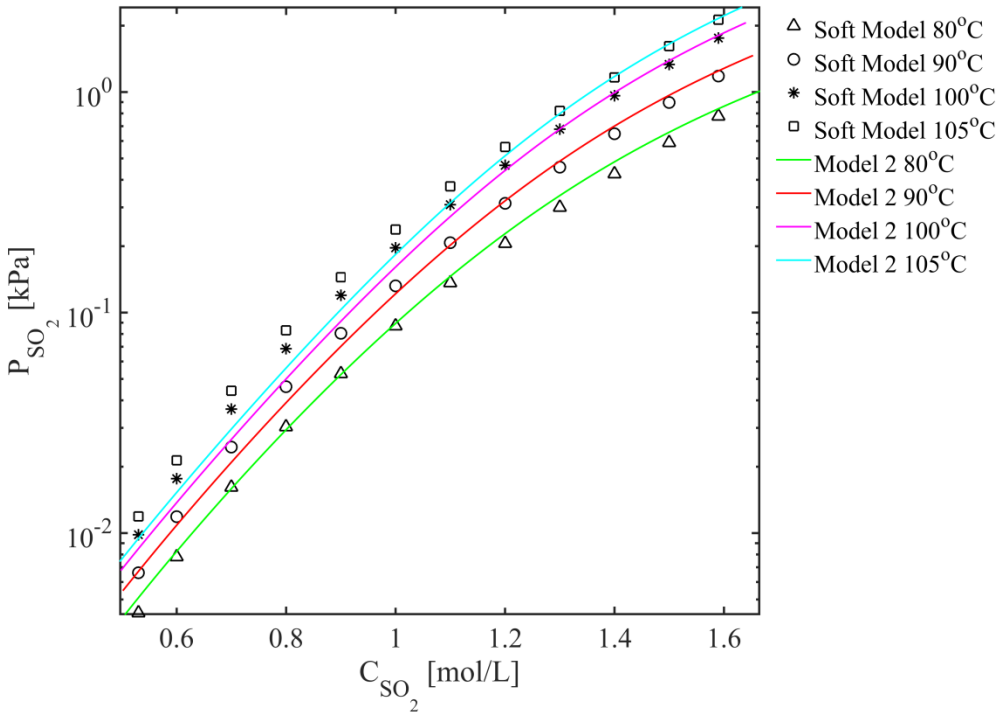

Figure E.6: The partial pressure of SO_2 as a function of the SO_2 concentration in the aqueous phosphate buffer solution 2.5/0.25/0.5. The average deviation of *model 2* is 12.0%.

Appendix F Stream Table: Absorption

Appendix F contains the stream tables that resulted when absorption of SO_2 was simulated in ASPEN Plus using operating conditions given in Table 2.1. The stream table resulted when simulating in the *standard model* and *model 1* is presented in Table F.1 and F.2, respectively. The stream names are equivalent to the stream names given in Figure 5.1.

Table F.1: The stream table resulted when absorption of SO_2 were simulated in the *standard model* in ASPEN Plus. 95% removal efficiency is achieved.

	Flue gas	**Clean gas**	**Lean Buffer**	**Rich Buffer**
Mole Flow [kmol/hr]				
SO_2	133.8	6.7	$3.63*10^{-3}$	0.114
H_2O	6913.0	6860.0	3964.3	3890.2
H_3PO_4	0	$1.71*10^{-15}$	$2.48*10^{-3}$	0.024
Na^+	0	0	669.8	669.8
H_3O^+	0	0	$1.48*10^{-4}$	$5.36*10^{-4}$
H_2PO4^-	0	0	136.8	260.4
HSO_3-	0	0	30.6	161.1
SO_3^{2-}	0	0	11.3	7.8
SO_4^{2-}	0	0	41.9	41.9
HPO_4^{2-}	0	0	198.0	74.4
PO_4^{3-}	0	0	$9.02*10^{-3}$	$6.17*10^{-4}$
CO_2	4186.7	4186.6	0	0.063
N_2	31216.2	31216.2	0	0.011
O_2	2165.3	2165.3	0	$1.34*10^{-3}$
C_{SO2} [kmol/m^3]	-	-	0.5	1.71
Total Flow [m^3/hr]	$1.20*10^6$	$1.21*10^6$	83.7	98.7
Temperature [°C]	55	59.1	55	60.2
Pressure [atm]	1	1	1	1
Vapour Fraction [-]	1	1	0	0
Liquid Fraction [-]	0	0	1	1

Table F.2: The stream table resulted when absorption of SO_2 were simulated in *model 1* in ASPEN Plus. 95% removal efficiency is achieved.

	Flue gas	**Clean gas**	**Lean Buffer**	**Rich Buffer**
Mole Flow [kmol/hr]				
SO_2	133.8	6.8	0.301	30.3
H_2O	6913.0	6911.7	3904.3	3808.4
H_3PO_4	0	1.8010^{-14}	0.027	1.3
Na^+	0	0	664.8	664.8
H_3O^+	0	0	5.09E-03	0.029
H_2PO4^-	0	0	127.3	220.5
HSO_3-	0	0	38.5	136.7
SO_3^{2-}	0	0	2.8	1.6
SO_4^{2-}	0	0	41.5	41.5
HPO_4^{2-}	0	0	204.8	110.6
PO_4^{3-}	0	0	0.2	1.3010^{-4}
CO_2	4186.7	4186.6	0	0.130
N_2	31216.2	31216.1	0	0.024
O_2	2165.3	2165.3	0	3.0410^{-3}
C_{SO2}[kmol/m^3]	-	-	0.5	1.77
Total Flow [m^3/hr]	$1.20*10^9$	$1.20*10^9$	83.1	95.2
Temperature [°C]	55	56.5	55	57.3
Pressure [atm]	1	1	1	1
Vapour Fraction [-]	0	1	1	0
Liquid Fraction [-]	1	0	0	1

Appendix G Stream Table: Regeneration

Appendix G contains stream tables that resulted when regeneration of SO_2 were simulated using the *standard model* in ASPEN Plus. The stream table for run 1 and 4 when solids are not taken into account is presented in Table G.1 and G.2. The stream table for run 4 when solids are accounted for is presented in G.3. The stream names are equivalent to the stream names given in Figure 5.5.

Table G.1: Stream table resulted for run 1 when regeneration of SO_2 was simulated in ASPEN Plus. 95% removal efficiency is achieved.

	Rich buffer	Rich3	Liquid	Vapour
Mole Flow [kmol/hr]				
SO_2	0.114	127.4	0.231	127.2
H_2O	3890.2	4017.5	688.3	3329.2
H_3PO_4	0.024	0.019	0.019	$2.72*10^{-15}$
Na^+	669.8	669.8	$6.7*10^{2}$	0
H_3O^+	$5.36*10^{-4}$	$3.95*10^{-5}$	$3.95*10^{-5}$	0
H_2PO4^-	260.4	125.4	125.4	0
HSO_3-	161.1	41.6	41.6	0
SO_3^{2-}	7.8	0.041	0.041	0
SO_4^{2-}	41.9	41.9	41.9	0
HPO_4^{2-}	74.4	209.5	209.5	0
PO_4^{3-}	$6.17*10^{-4}$	0.014	0.014	0
CO_2	0.063	0.063	$2.62*10^{-5}$	0.063
N_2	0.011	0.011	$1.42*10^{-8}$	0.011
O_2	$1.34*10^{-3}$	$1.34*10^{-3}$	$2.76*10^{-9}$	$1.34*10^{-3}$
m_{H2O} [kg/hr]	70083	72377	12401	59976
Total Flow [m^3/hr]	98.7	$1.1*10^{5}$	27.8	$1.1*10^{8}$
Temperature [°C]	60.2	125.8	125.8	125.8
Pressure [atm]	1	1	1	1
Vapour Fraction [-]	0	0.66	0	1
Liquid Fraction [-]	1	0.34	1	0

Table G.2: Stream table obtained for run 4 when regeneration of SO_2 was simulated in ASPEN Plus. 95% removal efficiency is achieved.

	Rich buffer	Rich3	Liquid	Vapour
Mole Flow [kmol/hr]				
SO_2	0.159	127.5	0.351	127.2
H_2O	5450.6	5578.0	1654.4	3923.6
H_3PO_4	0.034	0.032	0.032	$2.98*10^{-15}$
Na^+	938.4	938.4	938.4	0
H_3O^+	$7.51*10^{-4}$	$1.14*10^{-4}$	$1.14*10^{-4}$	0
H_2PO4^-	364.9	226.9	226.9	0
HSO_3-	225.7	109.0	109.0	0
SO_3^{2-}	11.0	0.335	0.335	0
SO_4^{2-}	58.7	58.7	58.7	0
HPO_4^{2-}	104.3	242.2	242.2	0
PO_4^{3-}	$8.65*10^{-4}$	0.012	0.012	0
CO_2	0.088	0.088	$3.87*10^{-5}$	0.088
N_2	0.015	0.015	$3.06*10^{-8}$	0.015
O_2	$1.87*10^{-3}$	$1.87*10^{-3}$	$6.01*10^{-9}$	$1.87*10^{-3}$
m_{H2O} [kg/hr]	98194	100489	29804	70685
Total Flow [m^3/hr]	$1.4*10^5$	$1.29*10^8$	57713	$1.29*10^8$
Temperature [°C]	60.2	118.5	118.5	118.5
Pressure [atm]	1	1	1	1
Vapour Fraction [-]	0	0.56	0	1
Liquid Fraction [-]	1	0.44	1	0

Table G.3: Stream table resulted for run 4 when regeneration of SO_2 was simulated in ASPEN Plus. Solids are accounted for and 95% removal efficiency is achieved.

	Rich buffer	Rich3	Liquid	Vapour
Mole Flow [kmol/hr]				
SO_2	0.159	130.9	3.6	127.2
H_2O	5450.7	3861.6	3457.4	404.3
H_3PO_4	0.033525	1.6	1.6	1.11E-14
Na^+	938.4	447.1	447.1	0
H_3O^+	0.001	0.018907	0.019	0
H_2PO4^-	364.9	220.3	220.3	0
HSO_3-	225.7	105.7	105.7	0
SO_3^{2-}	11.0	0.308	0.308	0
SO_4^{2-}	58.7	58.7	58.7	0
HPO_4^{2-}	104.3	1.6	1.6	0
PO_4^{3-}	8.65E-04	7.49E-07	7.49E-07	0
CO_2	0.088	0.088	1.53E-04	0.088
N_2	0.015	0.015	4.15E-07	0.015
O_2	1.87E-03	1.87E-03	8.54E-08	1.87E-03
$Na_2HPO_4*7H_2O$	0	245.7	245.7	0
$m_{Na2HPO4*7H2O}$ [kg/hr]	0	65857	65857	0
Total Flow [kg/hr]	1.90E+05	1.90E+05	1.75E+05	15438.34
Total Flow [m^3/hr]	1.38E+05	1.62E+07	1.25E+05	1.61E+07
Temperature [°C]	60.2	97.8	97.8	97.8
Pressure [atm]	1	1	1	1
Vapour Fraction [-]	0	0.105	0	1
Liquid Fraction [-]	1	0.847	0.946	0
Solid Fraction [-]	0	0.048	0.054	0

Appendix H Simulation of Absorption of SO_2 with Solids

To investigate whether it is possible to simulate the absorber column when solids are accounted for, the absorber was simulated as illustrated in Figure 5.1 in the *standard model* and with the operating conditions given in Table F.1. From the simulation it appeared that the absorber did only converge when the anhydrous were accounted for in the simulation, and not when the salts were accounted for. It was not found an answer to the convergence problem [38]. However, a possible option is to simplify the calculation in ASPEN Plus and still allow the user to see if there is potential salt precipitation (e.g. potential fouling issues). This setting can be made by changing the "salt precipitation handling" in ASPEN Plus to "ignore-check" and changing the max-salt-sat parameter to 0.1. When the salt precipitation handling is changed to ignore-check, salt reactions defined in the "chemistry" will not be considered during calculations of the column. However, the solubility index for the salts on each stage will be checked against the value of the solubility limit, i.e. max-salt-sat parameter. A warning will be issued if the solubility limit is exceeded. When the simulation was run, the warning shown in Figure H.1 appeared on the control panel.

```
*  WARNING
   SALTS MAY FORM ON SOME STAGES
   "NA2HP(S)" HAS THE HIGHEST SOLUBILITY INDEX (0.718410)
   ON STAGE "2" EXCEEDING THE SATURATION LIMIT (0.100000)
```

Figure H.1: Warning given on the control panel when simulating the absorber column with solids in ASPEN Plus

The warning announced that $Na_2HPO_4*2H_2O$ might precipitate if the concentration of the component were higher. The component would have precipitated if the solubility index was above 1.